Stem Cell Reports
Article

ISSCR

OPEN ACCESS

Human iPSC-Derived Neuronal Model of Tau-A152T Frontotemporal Dementia Reveals Tau-Mediated Mechanisms of Neuronal Vulnerability

M. Catarina Silva,[1] Chialin Cheng,[1] Waltraud Mair,[2] Sandra Almeida,[3] Helen Fong,[4] M. Helal U. Biswas,[3] Zhijun Zhang,[3] Yadong Huang,[4] Sally Temple,[5] Giovanni Coppola,[6] Daniel H. Geschwind,[6] Anna Karydas,[7] Bruce L. Miller,[7] Kenneth S. Kosik,[8] Fen-Biao Gao,[3] Judith A. Steen,[2] and Stephen J. Haggarty[1,*]

[1]Department of Neurology, Chemical Neurobiology Laboratory, Center for Human Genetic Research, Massachusetts General Hospital and Harvard Medical School, Boston, MA 02114, USA
[2]Department of Neurology, F.M. Kirby Neurobiology Center, Boston Children's Hospital, Harvard Medical School, Boston, MA 02115, USA
[3]Department of Neurology, University of Massachusetts Medical School, Worcester, MA 01655, USA
[4]Departments of Neurology and Pathology, Gladstone Institute of Neurological Disease, University of California, San Francisco, CA 94158, USA
[5]Neural Stem Cell Institute, Regenerative Research Foundation, Rensselaer, NY 12144, USA
[6]Departments of Neurology and Psychiatry and Biobehavioral Sciences, Semel Institute for Neuroscience and Human Behavior, University of California, Los Angeles, CA 90024, USA
[7]Department of Neurology, Memory and Aging Center, University of California, San Francisco, CA 94158, USA
[8]Department of Molecular, Cellular and Developmental Biology, Neuroscience Research Institute, University of California, Santa Barbara, CA 93106, USA
*Correspondence: shaggarty@mgh.harvard.edu
http://dx.doi.org/10.1016/j.stemcr.2016.08.001

SUMMARY

Frontotemporal dementia (FTD) and other tauopathies characterized by focal brain neurodegeneration and pathological accumulation of proteins are commonly associated with tau mutations. However, the mechanism of neuronal loss is not fully understood. To identify molecular events associated with tauopathy, we studied induced pluripotent stem cell (iPSC)-derived neurons from individuals carrying the tau-A152T variant. We highlight the potential of in-depth phenotyping of human neuronal cell models for pre-clinical studies and identification of modulators of endogenous tau toxicity. Through a panel of biochemical and cellular assays, A152T neurons showed accumulation, redistribution, and decreased solubility of tau. Upregulation of tau was coupled to enhanced stress-inducible markers and cell vulnerability to proteotoxic, excitotoxic, and mitochondrial stressors, which was rescued upon CRISPR/Cas9-mediated targeting of tau or by pharmacological activation of autophagy. Our findings unmask tau-mediated perturbations of specific pathways associated with neuronal vulnerability, revealing potential early disease biomarkers and therapeutic targets for FTD and other tauopathies.

INTRODUCTION

Frontotemporal dementia (FTD) refers to a group of neurodegenerative diseases caused by focal but progressive neuronal loss, astrogliosis, and spongiosis in the frontal and temporal cortices associated with abnormal intracellular accumulation of proteins, most commonly tau or TDP43 (TAR DNA-binding protein 43) (Karageorgiou and Miller, 2014; Neumann et al., 2015). Currently there are no effective disease-modifying therapies for FTD, making the treatment and prevention of FTD an area of significant unmet medical need.

Tau is expressed ubiquitously in the brain and locates predominantly in neuronal axons, where it regulates microtubule polymerization and guides the transport of proteins and organelles (Kosik et al., 1989; Morris et al., 2011). Alternative splicing of *MAPT* exons 2, 3, and 10 originates six tau isoforms that differ from one another by 29- or 58-amino-acid inserts at the N terminus, and by the presence of either three (3R-tau) or four (4R-tau) tandem-repeat sequences at the C terminus. Tau function and localization are regulated by post-translational modifications (PTMs); for example, phosphorylation, acetylation, and proteolysis (Johnson and Stoothoff, 2004; Min et al., 2010; Wang et al., 2009). In FTD, sporadic or autosomal dominant forms caused by *MAPT* mutations, inclusions containing hyperphosphorylated tau (P-tau) are detected within neurons and glia of affected brain regions.

Although these inclusions are key pathological features, the events leading to neuronal loss may start even earlier, but the tau species and precise molecular events causing cell death are poorly understood. Therefore it is crucial to investigate the early molecular events of disease, such as alterations in tau biochemistry and affected cellular pathways (Gerson et al., 2014; Johnson and Stoothoff, 2004). In this context, human induced pluripotent stem cell (iPSC)-derived neurons allow exploring the molecular basis of tau pathogenesis in a disease-relevant genetic background (Ehrlich et al., 2015; Haggarty et al., 2016; Iovino et al., 2015).

Here, we investigated the underlying molecular and cellular mechanisms of pathogenicity associated with the rare tau variant A152T in a human neuronal context. Although the role of tau A152T in disease is still debated, it has been shown to affect tau function and PTMs, promote oligomerization and postmortem detection of inclusions, cause neuronal dysfunction independent of aggregation and neuroinflammation in animal models,

and increase significantly the risk for FTD and other neurodegenerative diseases (Coppola et al., 2012; Kara et al., 2012; Labbe et al., 2015; Lee et al., 2013; Maeda et al., 2016; Decker et al., 2016; Pir et al., 2016; Sydow et al., 2016). We utilized iPSCs derived from A152T carriers and derived neural progenitor cells (NPCs) and differentiated neuronal cells (Figure 1A). These cells represent ex vivo models of human neurons, with tau expression at endogenous physiologically relevant levels and in the context of the genomic background associated with disease. Overall, our results reveal potential targets for disease-modifying therapeutics to affect FTD and other tauopathies.

RESULTS

Human iPSC Lines

Cells from two individuals carrying the *MAPT* heterozygous variant A152T (c.1407G > A; NCBI RefSeq NM_001123066; rs143624519) were studied. The first individual was diagnosed with a form of FTD, progressive supranuclear palsy, at the time of skin biopsy (FTD19, Table S1), whose iPSCs were generated using standard retroviral vectors and the Yamanaka factors OCT3/4, SOX2, KLF4, and c-MYC (Biswas et al., 2016). The second was an asymptomatic individual (Tau6, Table S1) whose iPSCs and neuronal phenotypes have been in part characterized by Fong et al. (2013). Two age-matched individuals were also included as non-mutant controls: 8330-8 (Sheridan et al., 2011) and CTR2-L17 (Almeida et al., 2012). Two iPSC clones from the first A152T carrier (19-L3, 19-L5), one clone from the second A152T carrier (Tau6-1), and two control iPSC clones (8330-8 and CTR2-L17) were selected for further studies (Table S1).

All iPSCs had typical characteristics of PSCs (Biswas et al., 2016; Fong et al., 2013), including: colony-type morphology; expression of the stem cell surface marker SSEA-4 and pluripotency transcription factors OCT4/POU5F1 and NANOG (Figure S1A); elevated expression of endogenous *OCT4/POU5F1*, *NANOG*, and the zinc-finger protein pluripotency marker *ZFP42/REX1*, relative to the corresponding fibroblasts (Figure S1B); and ability for iPSC in vitro formation of embryoid bodies (EBs) and spontaneous differentiation of EBs into the three germ layers ectoderm (*TUJ1* expression), mesoderm (*SMA* expression), and endoderm (*AFP* expression) (Figure S1C) (Itskovitz-Eldor et al., 2000). Sanger sequencing of the *MAPT* locus confirmed the c.1407G > A mutation in A152T iPSCs (Figure S1D). Preservation of normal karyotype was confirmed (Figure S1E). Based on cell proliferation, morphology, and ability to remain undifferentiated in culture over >50 passages, there were no qualitative differences between control and A152T iPSCs.

Derivation and Characterization of Human NPCs

NPC lines were generated from iPSCs through isolation of neural rosettes (Nemati et al., 2011; Ungrin et al., 2008) (Table S1). Newly generated NPCs were immunopositive for the neural stem cell markers Nestin, SOX2, and Musashi-1, and the neuroepithelial marker PAX6 (Figure 1B), and were maintained in proliferative state under defined growth media with EGF (epidermal growth factor) and FGF (fibroblast growth factor) (Figure 1A) (Nemati et al., 2011; Sheridan et al., 2011; Yuan et al., 2011). Based on proliferation, cell morphology, and viability, there were no qualitative differences between control and A152T NPCs (Figure 1B).

NPC Differentiation into Neurons

Based on an initial time-course analysis of NPC differentiation (Figures S2A–S2F), we examined cortical and synaptic markers in 5-week neurons from two control and two A152T lines. Both control and A152T neurons expressed markers of the cortical layers II–VI, with some variability between cell lines (Figure 1C) that was not correlated with *MAPT* genotype (Figure S2G), and comparable overall with a human anterior cingulate cortex (ACC) sample. Expression of cortical markers was also confirmed by immunofluorescence (IF) imaging of TBR1-, FEZF2-, CTIP2-, and FOXG1-positive neurons, with highest detection in the nucleus and cell body (Figures 1EI–1EIV). Expression of synaptic proteins PSD95, SYN1, and SYP was also detected at comparable levels in all neuronal cells (Figures 1D and S2H), with appreciable detection in neuronal processes but greater detection in the cell body, as expected at an early stage of neuronal maturity (Figures 1EV and 1EVI). NeuN is a neuronal-specific nuclear/perinuclear protein and MAP2 is a microtubule-associated protein, both utilized as neuronal markers (Figures 1D and 1EVIII). The diversity of neuronal cell types obtained from NPC differentiation was examined based on expression of specific markers. We detected glutamatergic neurons, which are highly affected in FTD (VGLUT1, Figures 1EVII and S3) (Huey et al., 2006), as well as cholinergic, GABAergic, dopaminergic/adrenergic, and serotonergic neurons, in addition to glia, with no detection of neural crest or cardiomyocyte lineage cells (Figure S3).

These results revealed that NPC-differentiated cells display neuron-specific morphology, and expression of protein markers reminiscent of in vivo neurogenesis and human cortical neurons. The variability captured between cell lines (Figures 1C and 1D) was mostly due to inherent differences between iPSC-derived clonal lines and was not correlated with *MAPT* genotype (Figures S2G and S2H).

Upregulation of Tau in A152T Neurons

FTD-associated *MAPT* mutations, including the variant A152T, have been shown to promote accumulation of tau

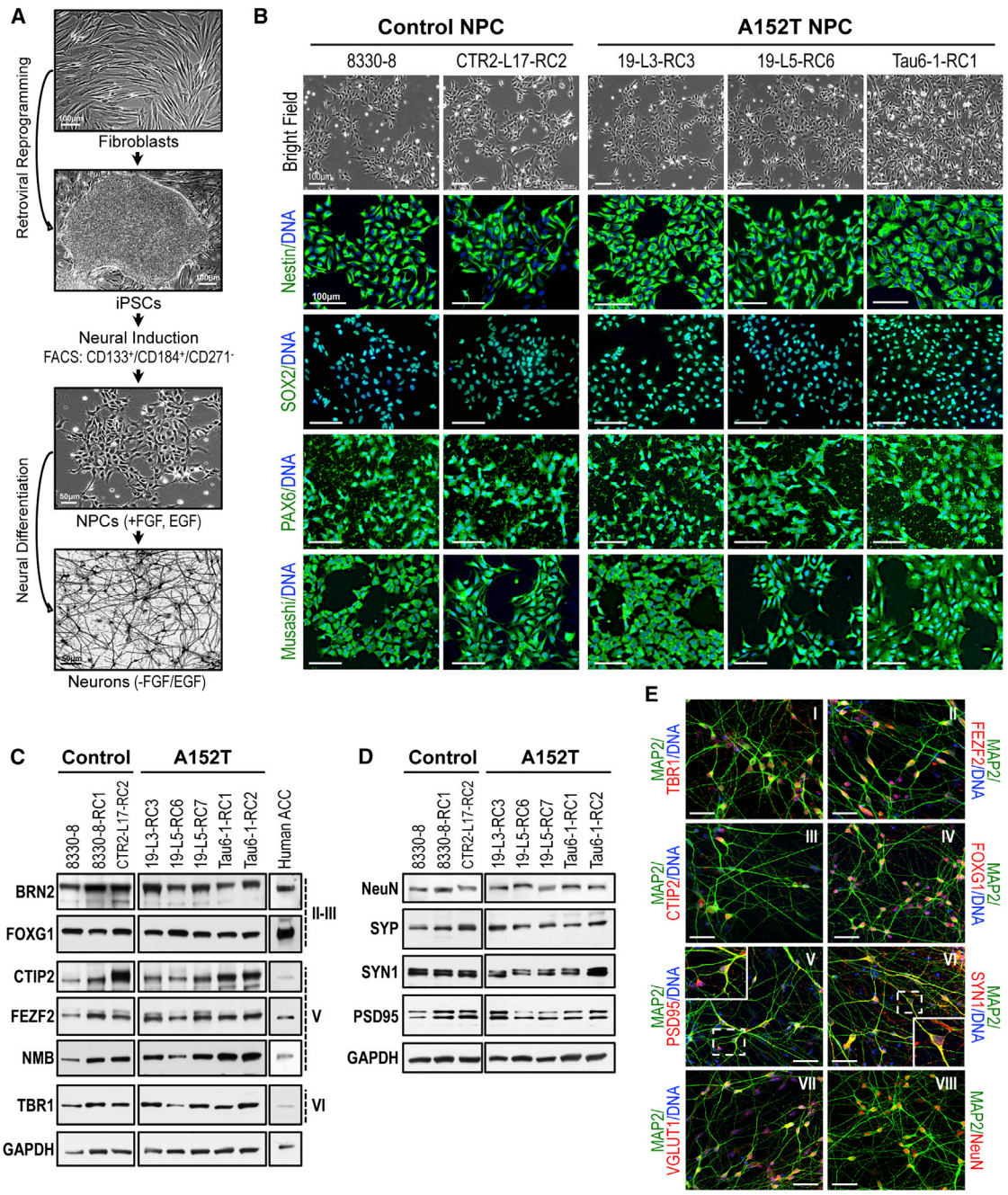

Figure 1. Human iPSC-Derived NPCs, and Synaptic and Cortical Markers in NPC-Derived Neurons

(A) Summary of the experimental strategy followed. See also Figure S1.

(B) Bright-field and IF analysis of NPC markers (green) in control and A152T lines. Scale bar, 100 μm.

(C and D) Western blot analysis of cortical layers II–III, V, and VI markers (C) and synaptic proteins (D), in 5-week control and A152T neurons. Human ACC is a positive control for cortical markers. GAPDH is the loading control. Samples ran in the same blot and are cropped for clarity ($n \geq 3$ independent experiments). See also Figure S2.

(E) IF analysis of cortical (I–IV), synaptic (V–VI), glutamatergic (VII), and neuronal (VIII) markers (red) in 5-week neurons (representative of control and A152T). Dotted insets correspond to zoomed-in images. Scale bars, 20 μm. See also Figure S3.

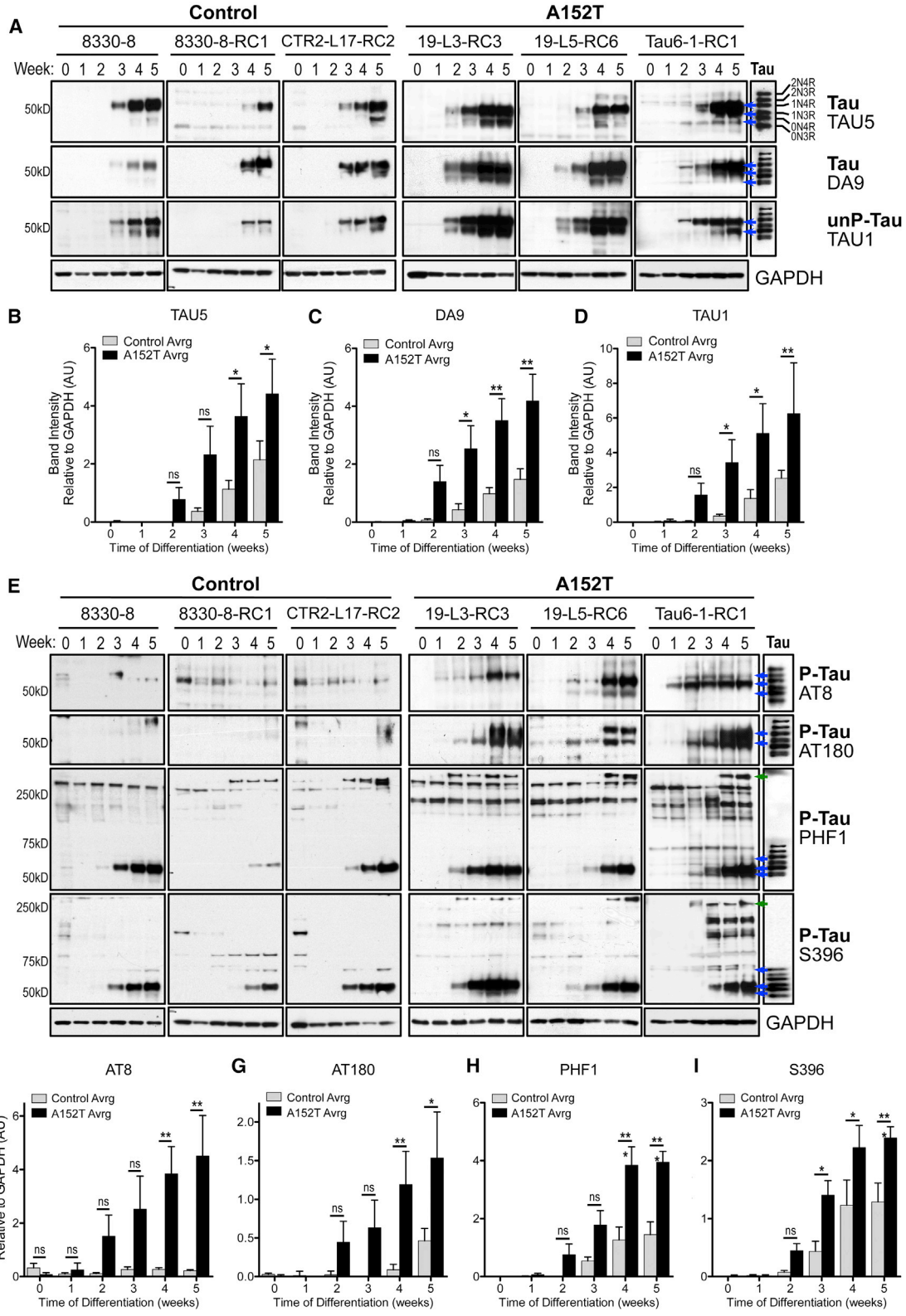

(legend on next page)

and neurodegeneration (Kara et al., 2012; Lee et al., 2013). To explore whether this is an early disease-relevant molecular event in A152T neurons, we started by examining tau protein levels and PTMs. To this end, we utilized three NPC lines derived from the FTD19 A152T carrier (19-L3-RC3, 19-L5-RC6, and 19-L5-RC7), two NPC lines from the Tau6 A152T carrier (Tau6-1-RC1 and Tau6-1-RC2), and three control NPC lines (8330-8, 8330-8-RC1, and CTR2-L17-RC2) (Table S1).

We first performed a time-course analysis of tau levels by western blot between proliferative state (week 0) and 5 weeks of differentiation, by employing a panel of seven tau and P-tau antibodies. By comparing averaged tau levels between controls and A152T lines, we detected a time-dependent increase in total tau levels (TAU5 and DA9 antibodies), with a more rapid tau upregulation in A152T neurons relative to control cells at 5 weeks of differentiation (Figures 2A–2C). These antibodies report on total protein independently of PTMs, which, together with alternative splicing isoforms, give rise to distinct molecular weight bands (Figure 2A, blue arrows). Recombinant human tau, consisting of a ladder of six tau isoforms without PTMs, was also included in the analysis to guide interpretation of band pattern, even though equivalent migration does not report on a particular endogenous tau isoform, given endogenous tau PTMs. TAU1 antibody that recognizes a form of non-P-tau (non-P-S199/S202/T205) corroborated overall tau upregulation in A152T neurons (Figures 2A and 2D). Further individual analysis of all cell lines at 5 weeks of differentiation revealed that, whereas FTD19-derived A152T neurons showed an upregulation of total tau, Tau6-1-derived neurons' total tau levels were more comparable with control after the same period of differentiation (Figures S4A and S4B).

Next, P-tau was examined with the antibodies AT8 (P-Ser202/Thr205), AT180 (P-Thr231/Ser235), PHF1 (P-Ser396/Ser404), and S396 (P-Ser396), which recognize phospho-epitopes associated with autosomal dominant forms of tauopathy (Davies, 2000; Goedert et al., 1995). The increase in P-tau levels was also time dependent and, whether analyzed between averaged controls versus A152T lines (Figures 2E–2I and S4B inset) or individually (Figures S4A and S4B), all A152T neurons showed an upregulation of P-tau relative to controls. In particular, AT8 and AT180 tau were barely detected in control neurons (Figures 2F and 2G). Only PHF1 and S396 antibodies revealed tau species of high molecular weight (HMW; >250 kDa) with specificity to A152T neurons (green arrows in Figures 2E and S4A), indicating the presence of oligomeric, hyper-P-tau at the Ser396/Ser404 epitope. Even with some variability among clonal lines, our findings suggest tau upregulation in A152T neurons, particularly in the form of P-tau (Figures 2E–2I and S4B). Semi-quantitative RT-PCR analysis revealed that *MAPT* expression was constant between control and A152T neurons (total *MAPT*, Figures S4C and S4D), and that 3R- and 4R-tau expression was also constant across cell lines, with higher 3R-tau levels, consistent with the immaturity of these 5-week neurons (Figures S4C and S4E) (Stein et al., 2014). These results suggest that upregulation of tau is a result of protein accumulation rather than altered gene expression. Subsequent studies are shown at 5 weeks of differentiation, unless noted otherwise, but all phenotypes were also validated up to 20 weeks of differentiation (not shown).

We next utilized IF to examine the subcellular distribution of tau and P-tau. A152T neurons, in particular FTD19-derived neurons, showed a stronger signal for total tau K9JA antibody in the cell body and neuronal processes relative to control (red in Figures 3I–3V). The distinction between A152T and control neurons was even more accentuated for P-tau PHF1 staining, which showed a weaker signal in control neurons, being almost absent in cell bodies, whereas A152T neurons showed strong PHF1 staining in cell body and neuronal processes (red in Figures 3VI–3X). Upon co-staining of tau (K9JA) and P-tau (PHF1), we observed a higher PHF1-to-K9JA (green-to-red) relative intensity in A152T neurons, with a stronger PHF1 signal in the cell body and neuronal processes of A152T neurons relative to control (Figures 3XI–3XV). We did not, however, detect foci-like tau staining, reminiscent of tau aggregates or tangles, and neurons were Thioflavin-S negative (not shown). Due to the high density of neuronal processes in these cultures, we were unable to use automated microscopy to accurately quantify subcellular tau levels.

Collectively, these results suggest that an early marker of A152T pathogenesis is an early and time-dependent

Figure 2. Time-Dependent Upregulation of Tau in A152T Neurons

(A and E) Total tau (A) and P-tau (E) expression by western blot analysis of up to 5-week differentiated neurons in control and A152T cell lines. Far-right panels show recombinant tau ladder (six tau isoforms, no PTMs); GAPDH is the loading control ($n \geq 3$ independent experiments). Arrows indicate bands quantified: blue for bands with corresponding migration to the tau ladder, green for HMW bands. Samples ran in same blot as far as possible.

(B–D and F–I) Semi-quantitative analysis of western blots in (A) and (E). Band intensities in a.u. relative to GAPDH, averaged (Avrg) across genotype (controls/gray, A152T/black) ± SEM. Two-way ANOVA and Bonferroni post test, $n \geq 3$ independent experiments: ns, not significant ($p > 0.05$); *$p < 0.05$, **$p < 0.01$.

See also Figure S4.

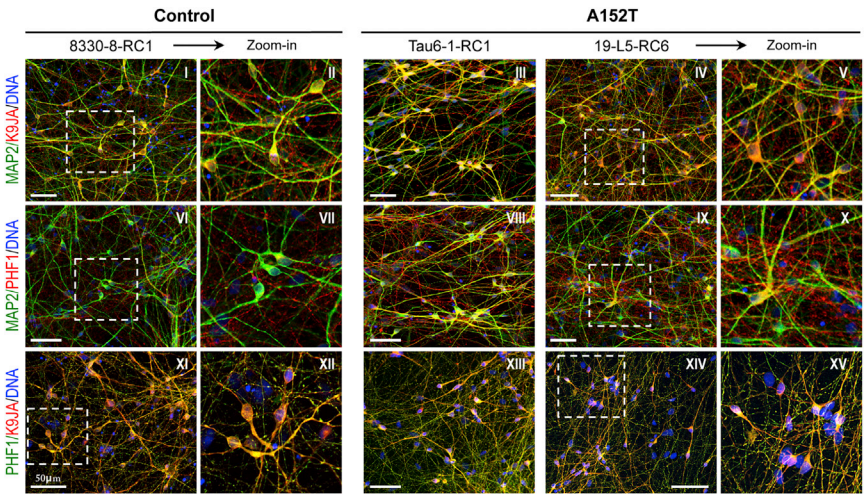

Figure 3. Upregulation of Tau in A152T Neurons by IF Analysis

Total tau (K9JA), P-tau (PHF1), and MAP2 by IF in control and A152T 5-week neurons. Dotted insets correspond to zoomed-in images shown on the right. Scale bars, 50 μm.

accumulation of tau, predominantly in the form of P-tau and oligomeric P-tau. IF corroborated the accumulation of tau/P-tau in A152T neurons, further revealing increased P-tau in neuronal processes and cell body of A152T neurons, consistent with somatodendritic redistribution, both important pathophysiological features of tauopathy, detected here as an early phenotype in patient-derived neurons in vitro (de Calignon et al., 2012; Fong et al., 2013; Li et al., 2011; Sydow et al., 2016).

Quantitative Analysis of Tau in Human Neurons by Mass Spectrometry

To corroborate our antibody-based results we employed FLEXITau, a mass spectrometry (MS)-based targeted assay for absolute quantification of tau protein levels and PTMs (Mair et al., 2016). A schematic of this methodology is shown in Figure 4A, and in-depth details have been described (Mair et al., 2016; Singh et al., 2009). FLEXITau absolute quantification of tau in control (8330-8-RC1) and A152T (19-L5-RC6) neurons at 5, 12, and 20 weeks of differentiation revealed upregulation of tau in A152T neurons, which was more pronounced at 20 weeks of differentiation (2.5-fold relative to control, average 28.5 fmol/μg and 11.4 fmol/μg protein lysate, respectively) (Figure 4B). Notably, the levels of tau in control neurons reached a plateau after 12 weeks, whereas A152T neurons showed a linear increase in tau levels up to 20 weeks of differentiation (Figure 4B, R^2 = 0.999; not shown), again indicative of aberrant tau accumulation in A152T neurons.

Differential Expression of Non-mutant and A152T Tau

Given the lack of variant-specific antibodies to date, all studies of expression of endogenous mutant tau have relied on the inference that the mutated allele is expressed. However, this hindrance precludes gaining an understanding of the ratio between non-mutant and mutant protein levels and misinterpretation of total protein levels, because gene mutations can alter protein stability and biochemical properties. Therefore, we used a targeted MS approach to measure non-mutant and variant tau protein levels in control and A152T neurons (LysC digest, Figure 4A). Shotgun tandem MS (MS/MS) analysis from LysC-digested control and A152T neurons identified the peptides $_{151}$I**A**TPRGAAPPGQK$_{163}$ (non-mutant) and $_{151}$I**T**TPRGAAPPGQK$_{163}$ (A152T) by specific peptide fragment spectra (Figure S5). For quantification of these peptides, we developed a targeted selected reaction monitoring (SRM) assay (Supplemental Experimental Procedures), which showed that in A152T neurons the levels of A152T tau are higher (56.6%) than non-mutant tau (43.4%), and this ratio stayed constant over the time points analyzed (Figure 4C), even though overall levels of total tau increased (Figure 4B). This is the first demonstration and quantification of allele-specific expression of a tau variant protein in a human iPSC-derived neuronal model.

Tau PTMs and Isoforms by Mass Spectrometry

FLEXITau MS analysis also enables the characterization of *MAPT* splicing and tau PTMs (Mair et al., 2016). This strategy relies on the quantification of unmodified tau peptides in a cell lysate relative to spiked-in stable isotope-labeled unmodified peptides derived from heavy-labeled tau protein. A reduction in cell lysate-measured light peptides is evidence of a "modification" in the endogenous tau peptide, and this modification can be a PTM, alternative splicing, or a mutation. We employed global FLEXITau analysis on 5-week neurons, using both trypsin and LysC samples to maximize sequence coverage (Figure 4A). The regions with the highest "modifications" were the exons that undergo alternative splicing (E2, E3, E10; Figure 4D). Within the sensitivity of our MS assay, the peptides

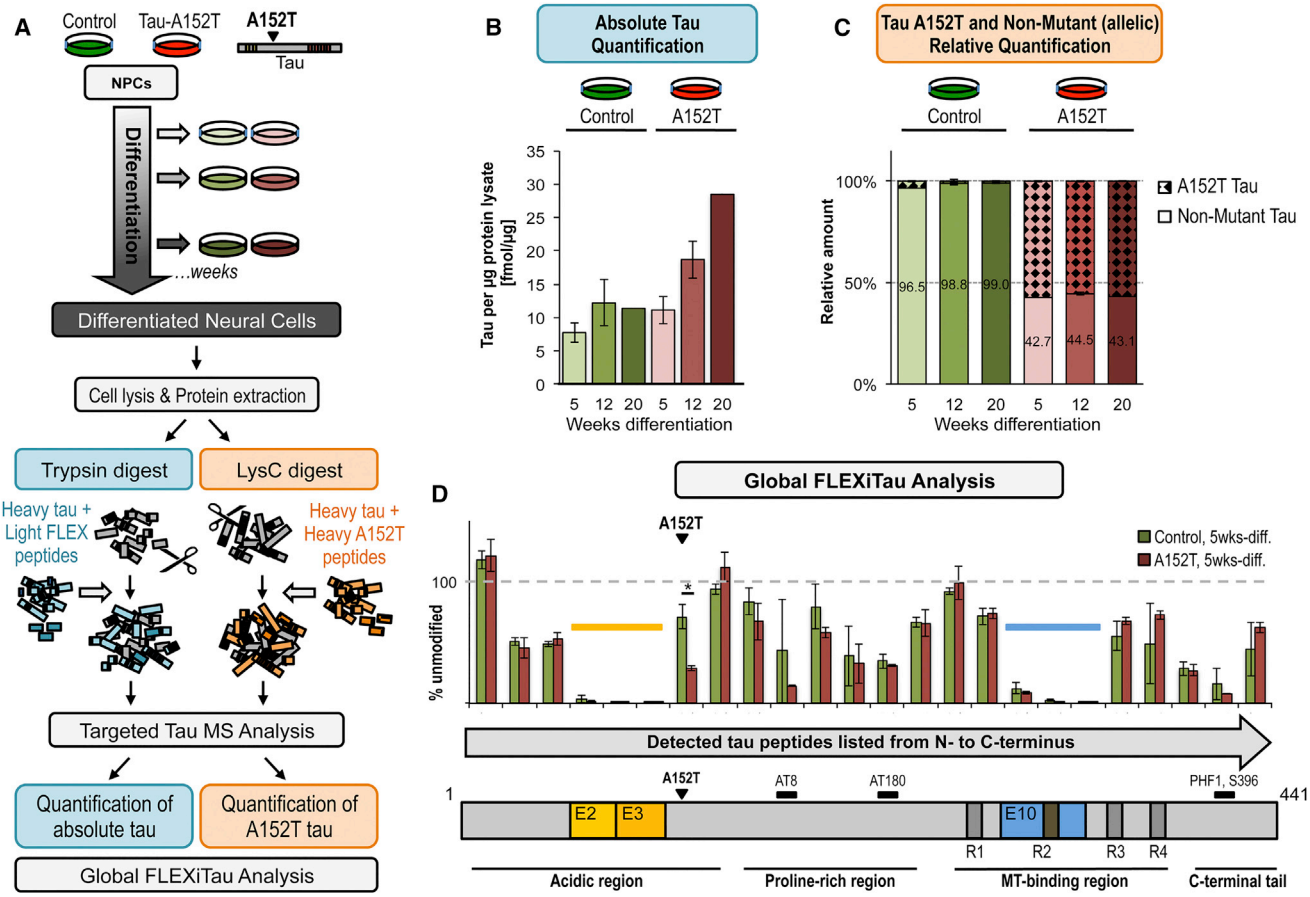

Figure 4. Tau Profile by MS Analysis

(A) Workflow for preparation of control (8330-8-RC1) and A152T (19-L5-RC6) samples for MS analysis.

(B) Quantification of total endogenous tau by FLEXITau. Shown is average tau in fmol/µg of protein lysate ± SD (n = 3, except n = 2 for week 20, see Experimental Procedures).

(C) Relative amount of endogenous non-mutant tau and A152T tau in control and A152T neurons (mean ± SD, n = 3, except n = 2 for week 20, see Experimental Procedures).

(D) Global quantitative peptide profile by FLEXITau, relative to full-length 2N4R-tau. Shown is the normalized amount of unmodified peptides relative to heavy tau protein standard (mean ± SD, n = 3 independent experiments). *p < 0.05, Student's t test.

See also Figure S5.

corresponding to E2 and E3 were not detected, whereas E10 (4R-tau) was detected by one peptide (Figure 4D), corroborating gene-expression analysis (Figures S4C and S4E) and predominance of the 0N3R isoform. FLEXITau also detected "modified" peptides within the proline-rich region and the C-terminal tail, probably corresponding to PTMs. The peptides harboring Ser202/Thr205 (AT8), Thr231/Ser235 (AT180), and Ser396/Ser404 (PHF1) epitopes showed a decrease in unmodified peptides, i.e., an increase in "modified" epitopes in A152T neurons relative to control ($p = 0.013$), consistent with increased P-tau (Figure 4D). As expected, in A152T neurons the non-mutant (unmodified) peptide that covers the A152 site ($_{151}$I**A**TPRGAAPPGQK$_{163}$) was only 47.5% of the corresponding peptide in control neurons, as the remaining "modified" peptide harbors to A152T variant (Figure 4D).

One possible mechanism for the variant A152T to alter tau function (Derisbourg et al., 2015) would be by creating a new threonine (Thr/T) P-site. To test this, we attempted to quantify the P-peptide $_{151}$Ip**T**TPRGAAPP GQK$_{163}$ by SRM analysis, using a synthetic heavy P-peptide as a reference. We were unable to detect the endogenous light counterpart within the sensitivity range of our SRM assay (as low as 2.5 fmol/µL of endogenous tau, not shown), suggesting that in human iPSC-derived neurons, the variant A152T is unlikely to create a new phosphorylation site or, if it does, it is phosphorylated to less than 2.5% occupancy.

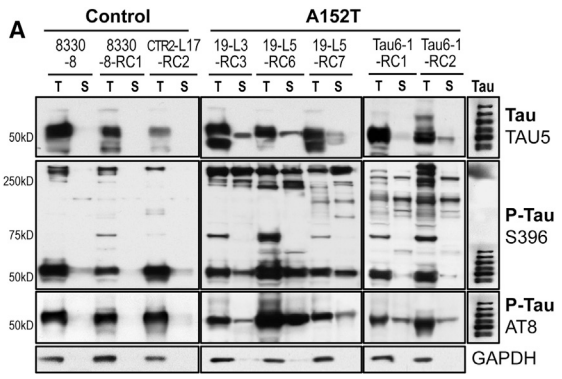

Figure 5. Detection of Insoluble Tau in A152T Neurons

(A) Western blot analysis of total tau (TAU5) and P-tau (S396, AT8) in Triton X (T)-soluble and Triton-X-insoluble SDS (S) fractions from 5-week neurons. GAPDH is the loading control.

(B) Semi-quantitative analysis of S-fraction band intensities from (A), relative to GAPDH in T-fraction (AU, arbitrary units). Values averaged between control, FTD19, and Tau6 lines (±SEM, n ≥ 3 independent experiments; *p ≤ 0.05, ***p ≤ 0.001, Student's t test).

Reduced Tau Solubility in A152T Neurons

To determine whether accumulation of P-tau led to the formation of protein species of reduced solubility, a hallmark of tauopathy, we tested tau protein differential solubility to Triton X-100 and SDS detergents (Guo and Lee, 2011, 2013; Kfoury et al., 2012). A152T neurons showed significantly more accumulation of Triton-insoluble total tau (TAU5) and P-tau (AT8, S396), i.e., SDS-fraction tau (S, Figure 5A). The HMW species (>250 kDa) detected by the P-tau S396 antibody showed a mixture of detergent-soluble and -insoluble tau in A152T neurons, but only Triton-soluble tau in control neurons. When comparing only the insoluble fractions (S), A152T neurons showed a preferential accumulation of P-tau, which was particularly accentuated in FTD19-derived neurons (Figure 5B). These results suggest that accumulation of tau in A152T neurons leads to the formation of species of reduced solubility, which is likely to negatively affect cellular function.

Affected Proteostasis in FTD Neurons

We examined whether upregulation of tau in A152T neurons affected proteostasis, which is kept by the concerted function of multiple pathways (Figure 6A), including the heat-shock response (HSR) and the ER and mitochondrial unfolded protein responses (UPR) that upregulate expression of molecular chaperones and other factors to prevent aberrant accumulation of proteins, and the ubiquitin proteasome system (UPS) and autophagy-lysosomal pathways responsible for clearance of these proteins (Balch et al., 2008; Wong and Cuervo, 2010). We asked whether these pathways were affected in A152T neurons by measuring pathway-specific components (Figure 6A, in blue). We examined 8-week differentiated neurons to take advantage of time-dependent accumulation of tau.

Relative to control, A152T neurons showed an increase in polyubiquitinated proteins (UBI1), which accumulate when UPS is disrupted, as well as an upregulation of autophagy markers (LC3B-II, ATG12/5, SQSTM1/p62, LAMP1, and LAMP2a), revealing activation of autophagy in A152T neurons (Figures 6B, 6F, 6D, and 6I). In contrast, there was no significant HSP70 chaperone family (HSP70, CHIP, HIP, and HOP) or HSP90 upregulation, suggesting no HSR induction (Figures 6C and 6G). To examine oxidative stress, we measured the levels of carbonylated proteins that accumulate in the cell by excessive protein oxidation (Figure 6D) (Dalle-Donne et al., 2003). A152T neurons showed a modest increase in stable 2,4-dinitrophenylhydrazone (DNP) proteins, suggesting disruption of proteostasis leading to oxidative stress ($p = 0.06$, Figure 6H). Finally, we examined UPR by measuring the ratios between the phospho-active forms and total levels of PERK, eIF2α, and IRE1α (Stutzbach et al., 2013), and the downstream targets CHOP and ER-HSP70 BiP (Figure 6A). Our results showed P-eIF2α/eIF2α and P-IRE1α/IRE1α upregulation in A152T neurons, with further increase in BiP and CHOP levels (Figure 6J). Even though we did not detect upregulation of P-PERK/PERK, CHOP is a downstream target of P-PERK and P-eIF2α, and transcriptional regulation cannot be excluded. Altogether, these results suggest that protein clearance and UPR are the most affected proteostasis pathways at the early stage of tau accumulation in an A152T iPSC-derived neuronal model.

Selective Vulnerability of A152T Neurons to Stress

Based upon the premise that tauopathy results from time-dependent cumulative cell damage due to buildup of toxic proteins, we asked whether accumulation of tau in A152T neurons was deleterious. If so, by "adding insult to injury" neurons affected by tau accumulation should have lower capacity to survive additional stress (Frost et al., 2015; Gidalevitz et al., 2010). With the goal of also identifying pathways that may be compromised by tau pathology, we treated 8-week neurons with pathway-specific chemical stressors and compared cell viability between A152T and control neurons (Figure 7A). These "stressors" included environmental toxins that inhibit the mitochondrial electron transport chain (ETC) complex I (rotenone and piericidin A) (Hoglinger et al., 2005; Hollerhage et al., 2014);

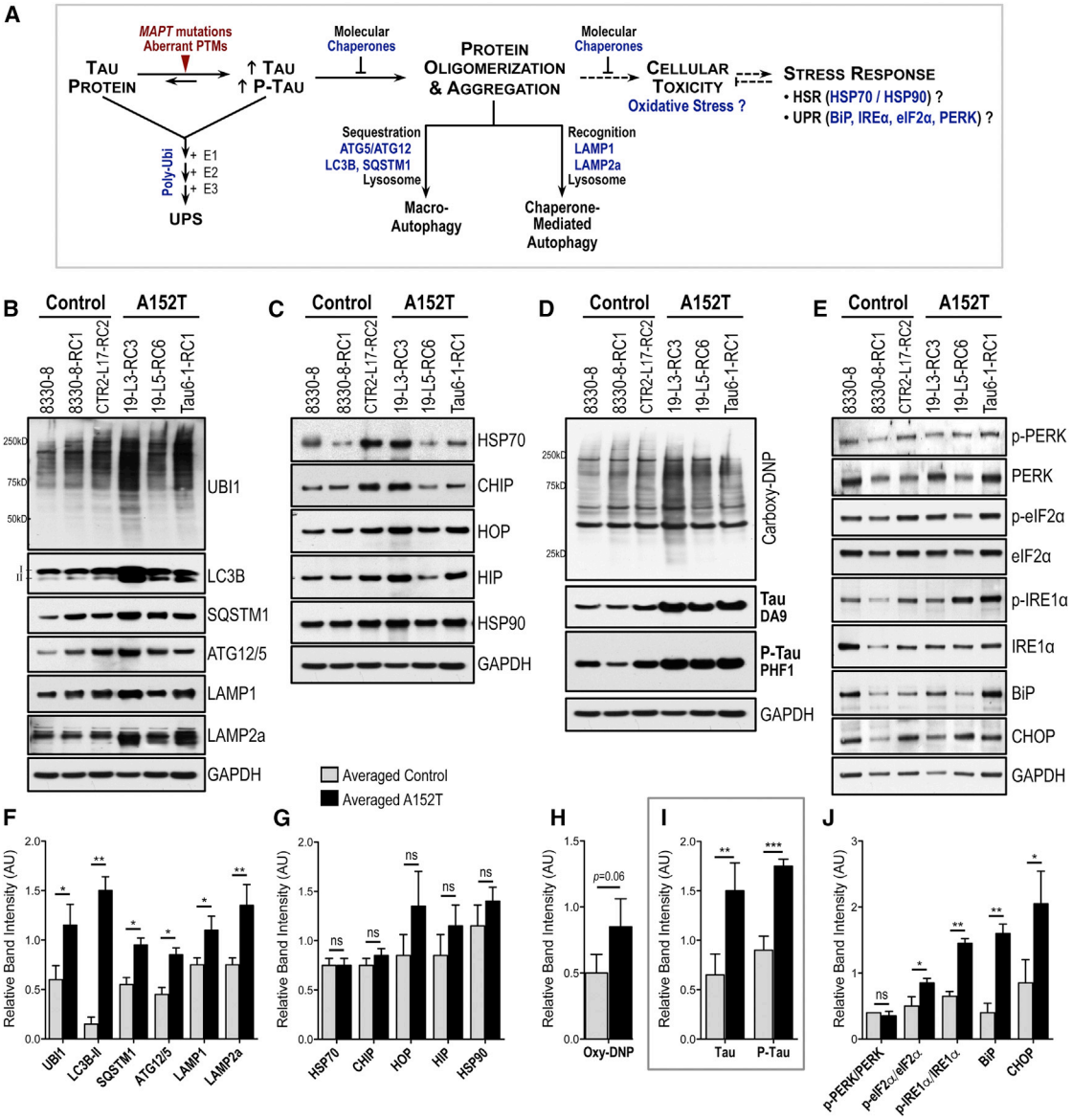

Figure 6. Enhanced Stress Markers in A152T Neurons

(A) Simplified representation of proteostasis pathways responsive to proteotoxic stress (blue denotes components measured).

(B–J) Western blot and semi-quantitative analysis, in 8-week control and A152T neurons, of: (B and F) polyubiquitinated (UBI1), macroautophagy (LC3B, SQSTM1/p62, ATG12-ATG5), and chaperone-mediated autophagy (LAMP1, LAMP2a) proteins; (C and G) molecular chaperones (HSP70, HSP90) and HSP70 co-chaperones (CHIP, HIP, HOP) of the HSR; (D and H) polycarbonylated proteins (DNP-derived); (E and J) UPR activation of PERK, eIF2α, and IRE1α, and downstream targets CHOP and BiP; (D and I) tau (DA9) and P-tau (PHF1). Shown is mean band intensity (±SD) relative to GAPDH; n = 3 independent experiments. Student's t test: *p < 0.05, **p < 0.01, ***p < 0.001; ns, not significant.

excitotoxic agonists of the glutamatergic AMPA and/or NMDA receptors (glutamate and NMDA) (Dong et al., 2009; Huey et al., 2006); and proteotoxic proteasome inhibitors (MG132 and epoxomicin) and A-β(1–42) amyloid peptide (a predominant component of amyloid plaques in Alzheimer's disease) (Roberson et al., 2007). To identify conditions whereby control and A152T neurons showed different survival, we started by performing a dose-dependent study in which compounds were added to neuronal cultures at different concentrations for 24 hr and cell viability was measured (Figures S6A–S6G). At the concentrations shown in Figure 7, stressor compounds had minimum impact in control neurons but caused a significant reduction in viability (<50% viable) of A152T neurons

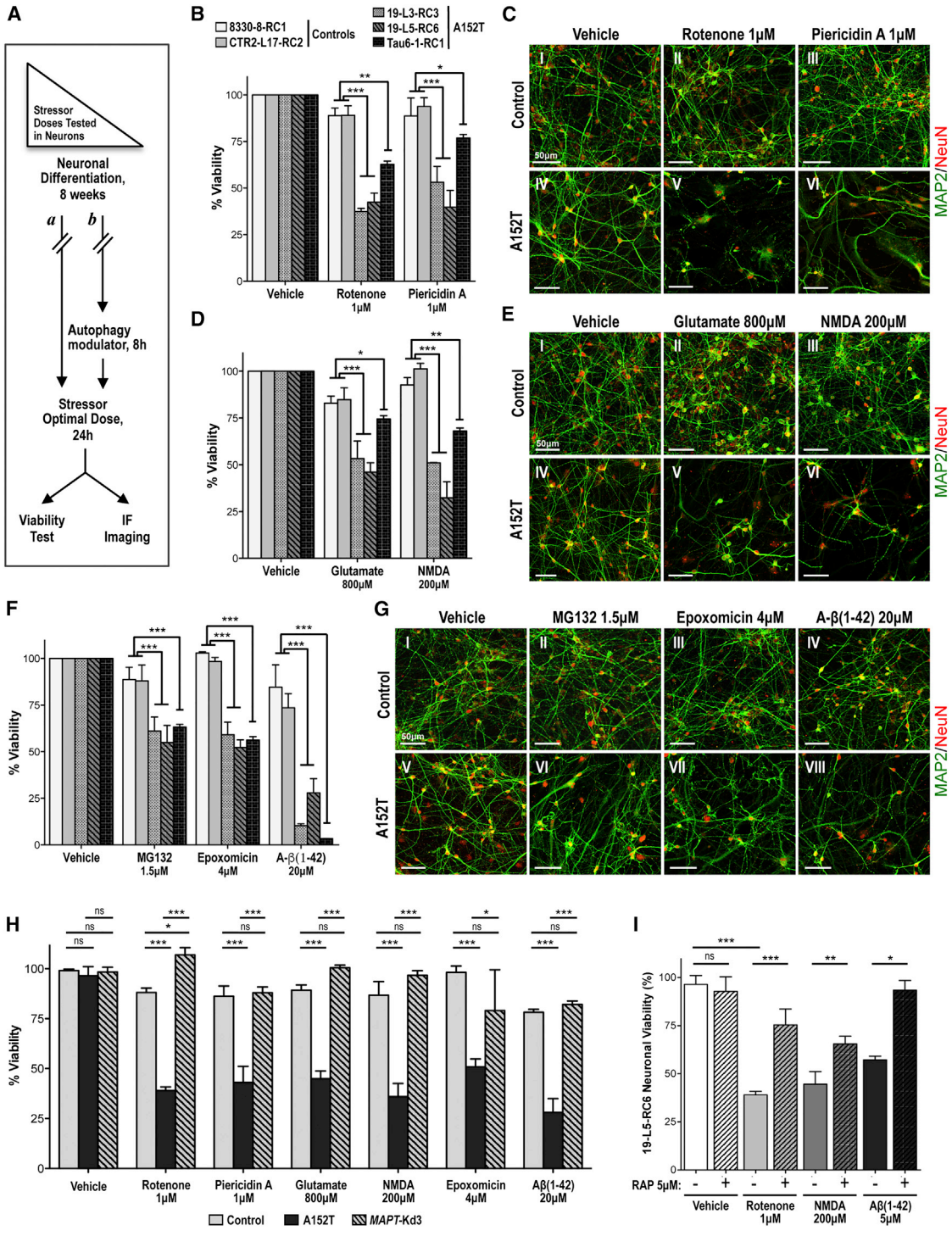

Figure 7. Increased Vulnerability to Stress in A152T Neurons Is Tau Dependent

(A) Overview of the stress vulnerability tests done in 8-week neurons (a) using high doses of stress, (b) pre-treating neurons with the autophagy inducer rapamycin, or by testing genetically engineered *MAPT*-Kd neurons.

(B, D, and F) Cell viability of 8-week neurons, treated with compounds for 24 hr. Values represent percent viability (±SEM) relative to vehicle-treated neurons. *$p < 0.05$, **$p < 0.01$, ***$p < 0.001$, two-way ANOVA and Bonferroni post test ($n \geq 3$ independent experiments).

(C, E, and G) IF analysis of neuronal integrity of control (CTR2-L17-RC2) and A152T (19-L3-RC3) neurons upon 24-hr treatment, based on MAP2/NeuN staining. Scale bars 50 μm.

(legend continued on next page)

(Figures 7B, 7D, and 7F). These effects were also detected by IF of MAP2 and NeuN as markers of neuronal integrity, where A152T neurons incubated with mitochondrial ETC inhibitors (Figure 7C), excitotoxins (Figure 7E), or proteotoxins (Figure 7G) showed selective cell loss. These results revealed a phenotype of cellular toxicity suggesting that tau/P-tau accumulation in A152T neurons is associated with increased stress vulnerability, consistent with the observation of altered stress-inducible markers (Figure 6).

Vulnerability of A152T Neurons to Stress Is Tau Dependent

To test the direct correlation between upregulation of tau in A152T neurons and increased vulnerability to stress, we examined whether downregulation of the "toxic" tau would be sufficient to rescue viability. First, we genomically engineered the A152T cell line 19-L5-RC6 with CRISPR/Cas9 constructs for targeting and disrupting expression of the *MAPT* gene (Hsu et al., 2014; Shalem et al., 2014). The resulting cell lines (19-L5-RC6;*MAPT*-Kd) revealed a sharp downregulation ($\geq$80%) of tau protein upon differentiation (Figures S6K and S6L), without detectable effect on neuronal integrity (Figures S6M and S2A) or cellular viability (Figure 7H). Remarkably, upon exposure to the cellular stressors that revealed vulnerability of the parental tau-A152T neurons, we observed a rescue of stress vulnerability in 8-week 19-L5-RC6;*MAPT*-Kd3 neurons, with viability increase to 90%–100%, similar to control (Figure 7H).

Second, we utilized the mTOR (mammalian target of rapamycin) inhibitor and autophagy activator rapamycin (Berger et al., 2006; Ozcelik et al., 2013). In control neurons, rapamycin downregulated tau by $\geq$50% via activation of the autophagy pathway, as shown by upregulation of the autophagosome marker LC3B-II (Figures S7N–S7P). We then pre-treated 8-week differentiated A152T neurons with rapamycin (8 hr) before exposure to stressor compounds (Figure 7A). Rapamycin-pre-treated A152T neurons showed a significant increase in cell viability relative to untreated neurons (Figure 7I). Consistent with the level of tau downregulation, rapamycin caused a milder but consistent rescue of viability compared with genetic knockdown (50% versus >80%, respectively).

Stress vulnerability tau dependence was further corroborated by testing the same stressors in 2-week neurons (Figures S6H–S6J), before tau accumulation, without a difference in survival between A152T and control neurons.

Altogether, these findings unequivocally demonstrate that accumulation of tau in A152T neurons is coupled to disruption of proteostasis and increased vulnerability to stress, early molecular events leading to neurodegeneration in tauopathy. Our study also demonstrates that endogenous tau-mediated cellular stress can be rescued by compounds that mediate tau clearance, which is of crucial relevance for the use of this cellular model for the development of therapeutics.

DISCUSSION

Human iPSC-derived neurons allow measurement of disease-relevant cellular and molecular phenotypes in a physiologically and genomically relevant context, potentially recapitulating the early stages of disease etiology, and allow direct testing of therapeutic targets and small molecules in a human neuronal environment (Almeida et al., 2012; Bilican et al., 2012; Ehrlich et al., 2015; Fong et al., 2013; Haggarty et al., 2016; Iovino et al., 2015; Wren et al., 2015). We took advantage of this system to investigate the early events of tau-A152T pathology that may be causal in FTD. Our findings contribute to mounting evidence, across studies of different tau mutations and across model systems, of tau-mediated molecular events associated with neurodegeneration, toward the identification of relevant therapeutic targets (Ehrlich et al., 2015; Fong et al., 2013; Iovino et al., 2015; Maeda et al., 2016; Decker et al., 2016; Pir et al., 2016; Sydow et al., 2016; Wren et al., 2015). We biochemically profiled neurons derived from control and A152T carriers, and report on a phenotyping platform for tau regarding protein levels, PTMs, and solubility. We demonstrate accumulation of endogenous tau/P-tau in A152T human neurons by multiple powerful methods. By western blot we found a significant upregulation of P-tau in all A152T neurons, whereas total tau upregulation was specific to the FTD19-derived neurons, consistent with previous reports (Fong et al., 2013; Sydow et al., 2016). This result might be a consequence of variability among individuals of the same *MAPT* genotype, and possibly the clinical outcome, but only future analysis of larger cohorts of cases could allow us to draw accurate conclusions. By MS analysis we verified upregulation of

(H) Cell viability of 8-week neurons upon 24-hr treatment. The genetically engineered line *MAPT*-Kd3 (19-L5-RC6;*MAPT*-Kd3) showed rescue of vulnerability to stress relative to A152T neurons. Percent viability (±SEM) is relative to vehicle-treated cells (100%). Two-way ANOVA and Bonferroni post test: *$p < 0.05$, ***$p < 0.001$; ns, not significant ($p > 0.05$) ($n \geq 3$ independent experiments).
(I) Rescue of A152T neuronal (19-L5-RC6) vulnerability to stress [24 hr of rotenone, NMDA, and Aβ(1–42)] by 8-hr pre-treatment of neuronal cultures with rapamycin (RAP, 5 μM). Percent viability (±SEM) is relative to vehicle-treated cells (100%). Student's t test: *$p < 0.05$, **$p < 0.01$, ***$p \leq 0.001$; ns, not significant ($p > 0.05$) ($n \geq 3$ independent experiments).
See also Figure S6.

absolute levels of endogenous tau in A152T neurons that became accentuated with time. By targeted MS, we demonstrated differential levels of tau A152T versus the non-mutant form in A152T neurons, which is relevant to the identification of "the toxic species." Even though this ratio (~60% versus 40%, respectively) was constant during the period of time tested (Figure 4C), the gradual increase in total tau (Figure 4B), suggests that this amount of tau-A152T is sufficient to cause some imbalance that leads to overall accumulation of tau.

By IF we detected an overall increase in tau in A152T neurons, with particular accumulation of P-tau in the cell body, consistent with somatodendritic redistribution of tau, as described for tauopathies and Alzheimer's disease (de Calignon et al., 2012; Fong et al., 2013; Li et al., 2011; Sydow et al., 2016). We did not detect A152T-specific changes in cell morphology, as reported in another A152T model (Fong et al., 2013), which may be due to differences in methodologies and line-specific variability. Nonetheless, the overall conclusion of tau accumulation, somatodendritic redistribution, and tau-mediated neuronal toxicity in A152T cells was a common observation, unmasked either by additional stress (Figure 7) or by genetic manipulation (A152T homozygous line in Fong et al., 2013). Taken together, these two studies are complementary by demonstrating that even with technical variability, key aspects in pre-clinical disease events were corroborated.

We also reveal here, for an FTD A152T proband-derived neuronal culture, a decrease in tau solubility, again most accentuated for P-tau. Although we did not detect tau puncta-like aggregates per se, Triton X-insoluble tau and the HMW species detected are consistent with oligomeric species of reduced solubility. Based on our findings we propose a model in which accumulation of P-tau and oligomeric tau of reduced solubility are early disease-causal phenotypes, consistent with other A152T animal models demonstrating tau-mediated toxicity independent of aggregation (Maeda et al., 2016; Pir et al., 2016).

To explore the mechanisms of tau-mediated toxicity, we focused on specific proteostasis pathways shown previously to be involved in tauopathy, including the HSP70/HSP90 chaperone machinery (Blair et al., 2013), UPR markers (Stutzbach et al., 2013), mitochondrial function and oxidative stress (Schulz et al., 2012), and autophagy (Wang and Mandelkow, 2012). We report on disruption of the UPS and autophagy pathways, in addition to UPR and oxidative stress induction, in A152T neurons. Disruption of protein clearance is a strong model for tau-mediated toxicity in neurodegeneration, and is consistent with the observed accumulation of total tau protein. Also consistent with our findings, a recent study identified alterations of the endosomal-lysosomal pathway associated with another tau mutation (Wren et al., 2015); yet another study identified LAMP1 and ubiquitin as cerebrospinal fluid markers of neurodegeneration, reinforcing the value of our system in the identification of tauopathy biomarkers (Heywood et al., 2015). In turn, mounting evidence points to UPR activation "in close connection with early stages of tau pathology" (Abisambra et al., 2013; Stoveken, 2013), and to mitochondrial dysfunction and vulnerability to oxidative stress as common aspects in iPSC-derived models of tauopathy (Ehrlich et al., 2015; Iovino et al., 2015).

Tau-mediated disruption of proteostasis was further revealed by increased sensitivity of A152T neurons to exogenous "stressors," unveiling toxicity phenotypes and pathways that may be affected in the early stages of tau pathology, offering a powerful method for phenotypic profiling of patient-derived neurons. Not all stressor compounds tested affected neuronal viability (not shown), revealing pathway-specific vulnerability. These phenotypes were tau dependent as shown by CRISPR/Cas9-mediated downregulation of *MAPT* expression in A152T neurons, which rescued neuronal stress vulnerability without affecting cell viability or integrity (Figures 7H and S6M). Most importantly, we demonstrate that stress vulnerability can be rescued pharmacologically by pre-treating neurons with the autophagy activator rapamycin, highlighting the value of this model for small-molecule screening. This is the first time, in a human neuronal cell context and with endogenous tau expression, that a compound has been shown to clear tau and consequently rescue toxicity. This result also further corroborates a model of tauopathy associated with disruption or inefficiency of protein clearance.

The results presented here are consistent with the proposition that the onset of cellular pathology in FTD occurs earlier than clinical manifestations, which has been corroborated by biomarker studies in Alzheimer's disease (Jack et al., 2013). By implementing a panel of biochemical and cellular assays, and a toolbox of compounds that reveal pathways affected by tau toxicity, we demonstrated the power of phenotypic characterization of patient-derived neuronal cells at the pre-clinical level, which is now suitable for mechanistic studies across *MAPT* genotypes. Finally, we show that endogenous tau phenotypes can be pharmacologically rescued, proving the suitability of our patient iPSC-derived neuronal model for screening therapeutic targets and disease-modifying agents relevant to FTD and other tauopathies.

EXPERIMENTAL PROCEDURES

iPSC, NPC, and Neuronal Cultures

Reprogramming, characterization, and maintenance of iPSCs, and NPC derivation have been described elsewhere (see Supplemental Experimental Procedures) (Zhao et al., 2012). NPCs were cultured

on polyornithine and laminin (POL)-coated plates, with DMEM/F12-B27 media supplemented with EGF, FGF, and heparin, and passaged with TrypLE (Life Technologies). Approval for work with human subjects' materials and iPSCs was obtained under IRB-approved protocols at Massachusetts General Hospital/Partners Healthcare (2009P002730) and University of California, San Francisco (10-00234). Neural differentiation was achieved by plating NPCs (passages 30–35) at a density of ~50,000 cells/cm^2 on POL plates, with DMEM/F12-B27 media only (no growth factors), and with $^1/_2$ medium change every 3–4 days.

Protein Analysis by Western Blot

Western blot analysis was performed using the Novex NuPAGE SDS-PAGE Gel System (Invitrogen) and standard immunoblotting techniques (see Supplemental Experimental Procedures).

LC-MS/MS Analysis

Absolute abundance of endogenous tau was determined using the FLEX peptide light-to heavy (L/H) ratio as recently described (Mair et al., 2016; Singh et al., 2009). The number of independent experiments was three; however, due to inherent challenges with long-term human neuronal differentiated cultures, there was a punctual necessity to pool samples for enough protein material at 20 weeks, for which n = 2 (Figures 4B–4D). See Supplemental Experimental Procedures for Expression and Purification of Heavy FLEXITau Standard, FLEXITau Sample Preparation and analysis, spectra analysis, data processing, and FLEXITau liquid chromatography (LC)-SRM measurements.

Analysis of Protein Solubility by Detergent Fractionation

The analysis was performed according to published protocols (see Supplemental Experimental Procedures).

MAPT Knockdown by CRISPR/Cas9 Genomic Engineering

The *MAPT* gene locus was targeted by the Tau CRISPR/Cas9 KO Plasmid (h) and Tau HDR Plasmid (h) (Santa Cruz Biotechnology sc-400136/sc-400136-HDR) in 19-L5-RC6 NPCs, according to the manufacturer's instructions (see Supplemental Experimental Procedures).

Compound Treatment and Viability Assays

Compound or vehicle alone was added directly onto the cellular medium. Viability was measured with the Alamar Blue Cell viability reagent (Life Technologies), according to the manufacturer's instructions. Readings were done in the EnVision Multilabel Plate Reader (PerkinElmer). For IF, fixed neurons image acquisition was done with the IN Cell Analyzer 6000 Cell Imaging System (GE Healthcare Life Sciences). For further details see Supplemental Experimental Procedures.

SUPPLEMENTAL INFORMATION

Supplemental Information includes Supplemental Experimental Procedures, six figures, and one table and can be found with this article online at http://dx.doi.org/10.1016/j.stemcr.2016.08.001.

AUTHOR CONTRIBUTIONS

Conceptualization, M.C.S., C.C., W.M., B.L.M., K.S.K., J.A.S., and S.J.H. Methodology, M.C.S., C.C., W.M., S.A., H.F., and S.J.H. Investigation, M.C.S., C.C., W.M., S.A., H.F., and S.J.H. Writing – Original Draft, M.C.S., W.M., S.T., D.H.G., J.A.S., and S.J.H. Writing – Review & Editing, M.C.S., C.C., S.A., Y.H., S.T., G.C., D.H.G., F.B.G., J.A.S., and S.J.H. Funding Acquisition, M.C.S., C.C., B.L.M., K.S.K., J.A.S., and S.J.H. Resources, S.A., H.F., H.U.B., Z.Z., Y.H., S.T., A.K., B.L.M., K.S.K., F.B.G., J.A.S., and S.J.H. Supervision, J.A.S. and S.J.H.

ACKNOWLEDGMENTS

We thank the Tau Consortium for funding, continued support, and helpful discussions; members of the Haggarty laboratory for technical assistance and feedback on the manuscript content; Drs. Eva-Maria and Eckhard Mandelkow for discussions around the neurobiology and biochemistry of tau; Dr. Peter Davies for the generous contribution of antibodies; and the Stanley Medical Research Institute for brain tissue samples. Additional funding support came from AFTD, 1R21NS085487, Bluefield Project to Cure Frontotemporal Dementia, P50AG023501, and P01AG019724.

Received: March 28, 2016
Revised: July 27, 2016
Accepted: August 1, 2016
Published: September 1, 2016

REFERENCES

Abisambra, J.F., Jinwal, U.K., Blair, L.J., O'Leary, J.C., III, Li, Q., Brady, S., Wang, L., Guidi, C.E., Zhang, B., Nordhues, B.A., et al. (2013). Tau accumulation activates the unfolded protein response by impairing endoplasmic reticulum-associated degradation. J. Neurosci. *33*, 9498–9507.

Almeida, S., Zhang, Z., Coppola, G., Mao, W., Futai, K., Karydas, A., Geschwind, M.D., Tartaglia, M.C., Gao, F., Gianni, D., et al. (2012). Induced pluripotent stem cell models of progranulin-deficient frontotemporal dementia uncover specific reversible neuronal defects. Cell Rep. *2*, 789–798.

Balch, W.E., Morimoto, R.I., Dillin, A., and Kelly, J.W. (2008). Adapting proteostasis for disease intervention. Science *319*, 916–919.

Berger, Z., Ravikumar, B., Menzies, F.M., Oroz, L.G., Underwood, B.R., Pangalos, M.N., Schmitt, I., Wullner, U., Evert, B.O., O'Kane, C.J., et al. (2006). Rapamycin alleviates toxicity of different aggregate-prone proteins. Hum. Mol. Genet. *15*, 433–442.

Bilican, B., Serio, A., Barmada, S.J., Nishimura, A.L., Sullivan, G.J., Carrasco, M., Phatnani, H.P., Puddifoot, C.A., Story, D., Fletcher, J., et al. (2012). Mutant induced pluripotent stem cell lines recapitulate aspects of TDP-43 proteinopathies and reveal cell-specific vulnerability. Proc. Natl. Acad. Sci. USA *109*, 5803–5808.

Biswas, M.H.U., Almeida, S., Lopez-Gonzalez, R., Mao, W., Zhang, Z., Karydas, A., Geschwind, M.D., Biernat, J., Mandelkow, E.-M., Futai, K., Miller, B.L., and Gao, F.-B. (2016). MMP-9 and MMP-2 contribute to neuronal cell death in iPSC models of

frontotemporal dementia with MAPT mutations. Stem Cell Rep. *7*. http://dx.doi.org/10.1016/j.stemcr.2016.08.006.

Blair, L.J., Zhang, B., and Dickey, C.A. (2013). Potential synergy between tau aggregation inhibitors and tau chaperone modulators. Alzheimers Res. Ther. *5*, 41.

Coppola, G., Chinnathambi, S., Lee, J.J., Dombroski, B.A., Baker, M.C., Soto-Ortolaza, A.I., Lee, S.E., Klein, E., Huang, A.Y., Sears, R., et al. (2012). Evidence for a role of the rare p.A152T variant in MAPT in increasing the risk for FTD-spectrum and Alzheimer's diseases. Hum. Mol. Genet. *21*, 3500–3512.

Dalle-Donne, I., Rossi, R., Giustarini, D., Milzani, A., and Colombo, R. (2003). Protein carbonyl groups as biomarkers of oxidative stress. Clin. Chim. Acta *329*, 23–38.

Davies, P. (2000). Characterization and use of monoclonal antibodies to tau and paired helical filament tau. Methods Mol. Med. *32*, 361–373.

de Calignon, A., Polydoro, M., Suarez-Calvet, M., William, C., Adamowicz, D.H., Kopeikina, K.J., Pitstick, R., Sahara, N., Ashe, K.H., Carlson, G.A., et al. (2012). Propagation of tau pathology in a model of early Alzheimer's disease. Neuron *73*, 685–697.

Decker, J.M., Krüger, L., Sydow, A., Dennissen, F.J., Siskova, Z., Mandelkow, E., and Mandelkow, E.M. (2016). The Tau/A152T mutation, a risk factor for frontotemporal-spectrum disorders, leads to NR2B receptor-mediated excitotoxicity. EMBO Rep. *17*, 552–569.

Derisbourg, M., Leghay, C., Chiappetta, G., Fernandez-Gomez, F.J., Laurent, C., Demeyer, D., Carrier, S., Buee-Scherrer, V., Blum, D., Vinh, J., et al. (2015). Role of the Tau N-terminal region in microtubule stabilization revealed by new endogenous truncated forms. Sci. Rep. *5*, 9659.

Dong, X.X., Wang, Y., and Qin, Z.H. (2009). Molecular mechanisms of excitotoxicity and their relevance to pathogenesis of neurodegenerative diseases. Acta Pharmacol. Sin. *30*, 379–387.

Ehrlich, M., Hallmann, A.L., Reinhardt, P., Arauzo-Bravo, M.J., Korr, S., Ropke, A., Psathaki, O.E., Ehling, P., Meuth, S.G., Oblak, A.L., et al. (2015). Distinct neurodegenerative changes in an induced pluripotent stem cell model of frontotemporal dementia linked to mutant TAU protein. Stem Cell Rep. *5*, 83–96.

Fong, H., Wang, C., Knoferle, J., Walker, D., Balestra, M.E., Tong, L.M., Leung, L., Ring, K.L., Seeley, W.W., Karydas, A., et al. (2013). Genetic correction of tauopathy phenotypes in neurons derived from human induced pluripotent stem cells. Stem Cell Rep. *1*, 226–234.

Frost, B., Gotz, J., and Feany, M.B. (2015). Connecting the dots between tau dysfunction and neurodegeneration. Trends Cell Biol. *25*, 46–53.

Gerson, J.E., Castillo-Carranza, D.L., and Kayed, R. (2014). Advances in therapeutics for neurodegenerative tauopathies: moving toward the specific targeting of the most toxic tau species. ACS Chem. Neurosci. *5*, 752–769.

Gidalevitz, T., Kikis, E.A., and Morimoto, R.I. (2010). A cellular perspective on conformational disease: the role of genetic background and proteostasis networks. Curr. Opin. Struct. Biol. *20*, 23–32.

Goedert, M., Jakes, R., and Vanmechelen, E. (1995). Monoclonal antibody AT8 recognises tau protein phosphorylated at both serine 202 and threonine 205. Neurosci. Lett. *189*, 167–169.

Guo, J.L., and Lee, V.M. (2011). Seeding of normal Tau by pathological Tau conformers drives pathogenesis of Alzheimer-like tangles. J. Biol. Chem. *286*, 15317–15331.

Guo, J.L., and Lee, V.M. (2013). Neurofibrillary tangle-like tau pathology induced by synthetic tau fibrils in primary neurons over-expressing mutant tau. FEBS Lett. *587*, 717–723.

Haggarty, S.J., Silva, M.C., Cross, A., Brandon, N.J., and Perlis, R.H. (2016). Advancing drug discovery for neuropsychiatric disorders using patient-specific stem cell models. Mol. Cell Neurosci. *73*, 104–115.

Heywood, W.E., Galimberti, D., Bliss, E., Sirka, E., Paterson, R.W., Magdalinou, N.K., Carecchio, M., Reid, E., Heslegrave, A., Fenoglio, C., et al. (2015). Identification of novel CSF biomarkers for neurodegeneration and their validation by a high-throughput multiplexed targeted proteomic assay. Mol. Neurodegener. *10*, 64.

Hoglinger, G.U., Lannuzel, A., Khondiker, M.E., Michel, P.P., Duyckaerts, C., Feger, J., Champy, P., Prigent, A., Medja, F., Lombes, A., et al. (2005). The mitochondrial complex I inhibitor rotenone triggers a cerebral tauopathy. J. Neurochem. *95*, 930–939.

Hollerhage, M., Deck, R., De Andrade, A., Respondek, G., Xu, H., Rosler, T.W., Salama, M., Carlsson, T., Yamada, E.S., Gad El Hak, S.A., et al. (2014). Piericidin A aggravates Tau pathology in P301S transgenic mice. PLoS One *9*, e113557.

Hsu, P.D., Lander, E.S., and Zhang, F. (2014). Development and applications of CRISPR-Cas9 for genome engineering. Cell *157*, 1262–1278.

Huey, E.D., Putnam, K.T., and Grafman, J. (2006). A systematic review of neurotransmitter deficits and treatments in frontotemporal dementia. Neurology *66*, 17–22.

Iovino, M., Agathou, S., Gonzalez-Rueda, A., Del Castillo Velasco-Herrera, M., Borroni, B., Alberici, A., Lynch, T., O'Dowd, S., Geti, I., Gaffney, D., et al. (2015). Early maturation and distinct tau pathology in induced pluripotent stem cell-derived neurons from patients with MAPT mutations. Brain *138*, 3345–3359.

Itskovitz-Eldor, J., Schuldiner, M., Karsenti, D., Eden, A., Yanuka, O., Amit, M., Soreq, H., and Benvenisty, N. (2000). Differentiation of human embryonic stem cells into embryoid bodies compromising the three embryonic germ layers. Mol. Med. *6*, 88–95.

Jack, C.R., Jr., Knopman, D.S., Jagust, W.J., Petersen, R.C., Weiner, M.W., Aisen, P.S., Shaw, L.M., Vemuri, P., Wiste, H.J., Weigand, S.D., et al. (2013). Tracking pathophysiological processes in Alzheimer's disease: an updated hypothetical model of dynamic biomarkers. Lancet Neurol. *12*, 207–216.

Johnson, G.V., and Stoothoff, W.H. (2004). Tau phosphorylation in neuronal cell function and dysfunction. J. Cell Sci. *117*, 5721–5729.

Kara, E., Ling, H., Pittman, A.M., Shaw, K., de Silva, R., Simone, R., Holton, J.L., Warren, J.D., Rohrer, J.D., Xiromerisiou, G., et al. (2012). The MAPT p.A152T variant is a risk factor associated with tauopathies with atypical clinical and neuropathological features. Neurobiol. Aging *33*, 2231.e7–2231.e14.

Karageorgiou, E., and Miller, B.L. (2014). Frontotemporal lobar degeneration: a clinical approach. Semin. Neurol. *34*, 189–201.

Kfoury, N., Holmes, B.B., Jiang, H., Holtzman, D.M., and Diamond, M.I. (2012). Trans-cellular propagation of Tau aggregation by fibrillar species. J. Biol. Chem. *287*, 19440–19451.

Kosik, K.S., Orecchio, L.D., Bakalis, S., and Neve, R.L. (1989). Developmentally regulated expression of specific tau sequences. Neuron *2*, 1389–1397.

Labbe, C., Ogaki, K., Lorenzo-Betancor, O., Soto-Ortolaza, A.I., Walton, R.L., Rayaprolu, S., Fujioka, S., Murray, M.E., Heckman, M.G., Puschmann, A., et al. (2015). Role for the microtubule-associated protein tau variant p.A152T in risk of alpha-synucleinopathies. Neurology *85*, 1680–1686.

Lee, S.E., Tartaglia, M.C., Yener, G., Genc, S., Seeley, W.W., Sanchez-Juan, P., Moreno, F., Mendez, M.F., Klein, E., Rademakers, R., et al. (2013). Neurodegenerative disease phenotypes in carriers of MAPT p.A152T, a risk factor for frontotemporal dementia spectrum disorders and Alzheimer disease. Alzheimer Dis. Assoc. Disord. *27*, 302–309.

Li, X., Kumar, Y., Zempel, H., Mandelkow, E.M., Biernat, J., and Mandelkow, E. (2011). Novel diffusion barrier for axonal retention of Tau in neurons and its failure in neurodegeneration. EMBO J. *30*, 4825–4837.

Maeda, S., Djukic, B., Taneja, P., Yu, G.Q., Lo, I., Davis, A., Craft, R., Guo, W., Wang, X., Kim, D., et al. (2016). Expression of A152T human tau causes age-dependent neuronal dysfunction and loss in transgenic mice. EMBO Rep. *17*, 530–551.

Mair, W., Muntel, J., Tepper, K., Tang, S., Biernat, J., Seeley, W.W., Kosik, K.S., Mandelkow, E., Steen, H., and Steen, J.A. (2016). FLEXITau: quantifying post-translational modifications of tau protein in vitro and in human disease. Anal. Chem. *88*, 3704–3714.

Min, S.W., Cho, S.H., Zhou, Y., Schroeder, S., Haroutunian, V., Seeley, W.W., Huang, E.J., Shen, Y., Masliah, E., Mukherjee, C., et al. (2010). Acetylation of tau inhibits its degradation and contributes to tauopathy. Neuron *67*, 953–966.

Morris, M., Maeda, S., Vossel, K., and Mucke, L. (2011). The many faces of tau. Neuron *70*, 410–426.

Nemati, S., Hatami, M., Kiani, S., Hemmesi, K., Gourabi, H., Masoudi, N., Alaei, S., and Baharvand, H. (2011). Long-term self-renewable feeder-free human induced pluripotent stem cell-derived neural progenitors. Stem Cells Dev. *20*, 503–514.

Neumann, M., Kovacs, G.G., and Mackenzie, I.R.A. (2015). Neuropathology of frontotemporal dementia and related disorders. In Hodges' Frontotemporal Dementia, B.C. Dickerson, ed. (Cambridge University Press), pp. 165–184.

Ozcelik, S., Fraser, G., Castets, P., Schaeffer, V., Skachokova, Z., Breu, K., Clavaguera, F., Sinnreich, M., Kappos, L., Goedert, M., et al. (2013). Rapamycin attenuates the progression of tau pathology in P301S tau transgenic mice. PLoS One *8*, e62459.

Pir, G.J., Choudhary, B., Mandelkow, E., and Mandelkow, E.M. (2016). Tau mutant A152T, a risk factor for FTD/PSP, induces neuronal dysfunction and reduced lifespan independently of aggregation in a *C. elegans* tauopathy model. Mol. Neurodegener. *11*, 33.

Roberson, E.D., Scearce-Levie, K., Palop, J.J., Yan, F., Cheng, I.H., Wu, T., Gerstein, H., Yu, G.Q., and Mucke, L. (2007). Reducing endogenous tau ameliorates amyloid beta-induced deficits in an Alzheimer's disease mouse model. Science *316*, 750–754.

Schulz, K.L., Eckert, A., Rhein, V., Mai, S., Haase, W., Reichert, A.S., Jendrach, M., Muller, W.E., and Leuner, K. (2012). A new link to mitochondrial impairment in tauopathies. Mol. Neurobiol. *46*, 205–216.

Shalem, O., Sanjana, N.E., Hartenian, E., Shi, X., Scott, D.A., Mikkelsen, T.S., Heckl, D., Ebert, B.L., Root, D.E., Doench, J.G., et al. (2014). Genome-scale CRISPR-Cas9 knockout screening in human cells. Science *343*, 84–87.

Sheridan, S.D., Theriault, K.M., Reis, S.A., Zhou, F., Madison, J.M., Daheron, L., Loring, J.F., and Haggarty, S.J. (2011). Epigenetic characterization of the FMR1 gene and aberrant neurodevelopment in human induced pluripotent stem cell models of fragile X syndrome. PLoS One *6*, e26203.

Singh, S., Springer, M., Steen, J., Kirschner, M.W., and Steen, H. (2009). FLEXIQuant: a novel tool for the absolute quantification of proteins, and the simultaneous identification and quantification of potentially modified peptides. J. Proteome Res. *8*, 2201–2210.

Stein, J.L., de la Torre-Ubieta, L., Tian, Y., Parikshak, N.N., Hernandez, I.A., Marchetto, M.C., Baker, D.K., Lu, D., Hinman, C.R., Lowe, J.K., et al. (2014). A quantitative framework to evaluate modeling of cortical development by neural stem cells. Neuron *83*, 69–86.

Stoveken, B.J. (2013). Tau pathology as a cause and consequence of the UPR. J. Neurosci. *33*, 14285–14287.

Stutzbach, L.D., Xie, S.X., Naj, A.C., Albin, R., Gilman, S., PSP Genetics Study Group, Lee, V.M., Trojanowski, J.Q., Devlin, B., and Schellenberg, G.D. (2013). The unfolded protein response is activated in disease-affected brain regions in progressive supranuclear palsy and Alzheimer's disease. Acta Neuropathol. Commun. *1*, 31.

Sydow, A., Hochgrafe, K., Konen, S., Cadinu, D., Matenia, D., Petrova, O., Joseph, M., Dennissen, F.J., and Mandelkow, E.M. (2016). Age-dependent neuroinflammation and cognitive decline in a novel Ala152Thr-Tau transgenic mouse model of PSP and AD. Acta Neuropathol. Commun. *4*, 17.

Ungrin, M.D., Joshi, C., Nica, A., Bauwens, C., and Zandstra, P.W. (2008). Reproducible, ultra high-throughput formation of multicellular organization from single cell suspension-derived human embryonic stem cell aggregates. PLoS One *3*, e1565.

Wang, Y., and Mandelkow, E. (2012). Degradation of tau protein by autophagy and proteasomal pathways. Biochem. Soc. Trans. *40*, 644–652.

Wang, Y., Martinez-Vicente, M., Kruger, U., Kaushik, S., Wong, E., Mandelkow, E.M., Cuervo, A.M., and Mandelkow, E. (2009). Tau fragmentation, aggregation and clearance: the dual role of lysosomal processing. Hum. Mol. Genet. *18*, 4153–4170.

Wong, E., and Cuervo, A.M. (2010). Integration of clearance mechanisms: the proteasome and autophagy. Cold Spring Harb. Perspect. Biol. *2*, a006734.

Wren, M.C., Zhao, J., Liu, C.C., Murray, M.E., Atagi, Y., Davis, M.D., Fu, Y., Okano, H.J., Ogaki, K., Strongosky, A.J., et al. (2015).

Frontotemporal dementia-associated N279K tau mutant disrupts subcellular vesicle trafficking and induces cellular stress in iPSC-derived neural stem cells. Mol. Neurodegener. *10*, 46.

Yuan, S.H., Martin, J., Elia, J., Flippin, J., Paramban, R.I., Hefferan, M.P., Vidal, J.G., Mu, Y., Killian, R.L., Israel, M.A., et al. (2011). Cell-surface marker signatures for the isolation of neural stem cells, glia and neurons derived from human pluripotent stem cells. PLoS One *6*, e17540.

Zhao, W.N., Cheng, C., Theriault, K.M., Sheridan, S.D., Tsai, L.H., and Haggarty, S.J. (2012). A high-throughput screen for Wnt/beta-catenin signaling pathway modulators in human iPSC-derived neural progenitors. J. Biomol. Screen. *17*, 1252–1263.

Stem Cell Reports, Volume *7*

Supplemental Information

Human iPSC-Derived Neuronal Model of Tau-A152T Frontotemporal Dementia Reveals Tau-Mediated Mechanisms of Neuronal Vulnerability

M. Catarina Silva, Chialin Cheng, Waltraud Mair, Sandra Almeida, Helen Fong, M. Helal U. Biswas, Zhijun Zhang, Yadong Huang, Sally Temple, Giovanni Coppola, Daniel H. Geschwind, Anna Karydas, Bruce L. Miller, Kenneth S. Kosik, Fen-Biao Gao, Judith A. Steen, and Stephen J. Haggarty

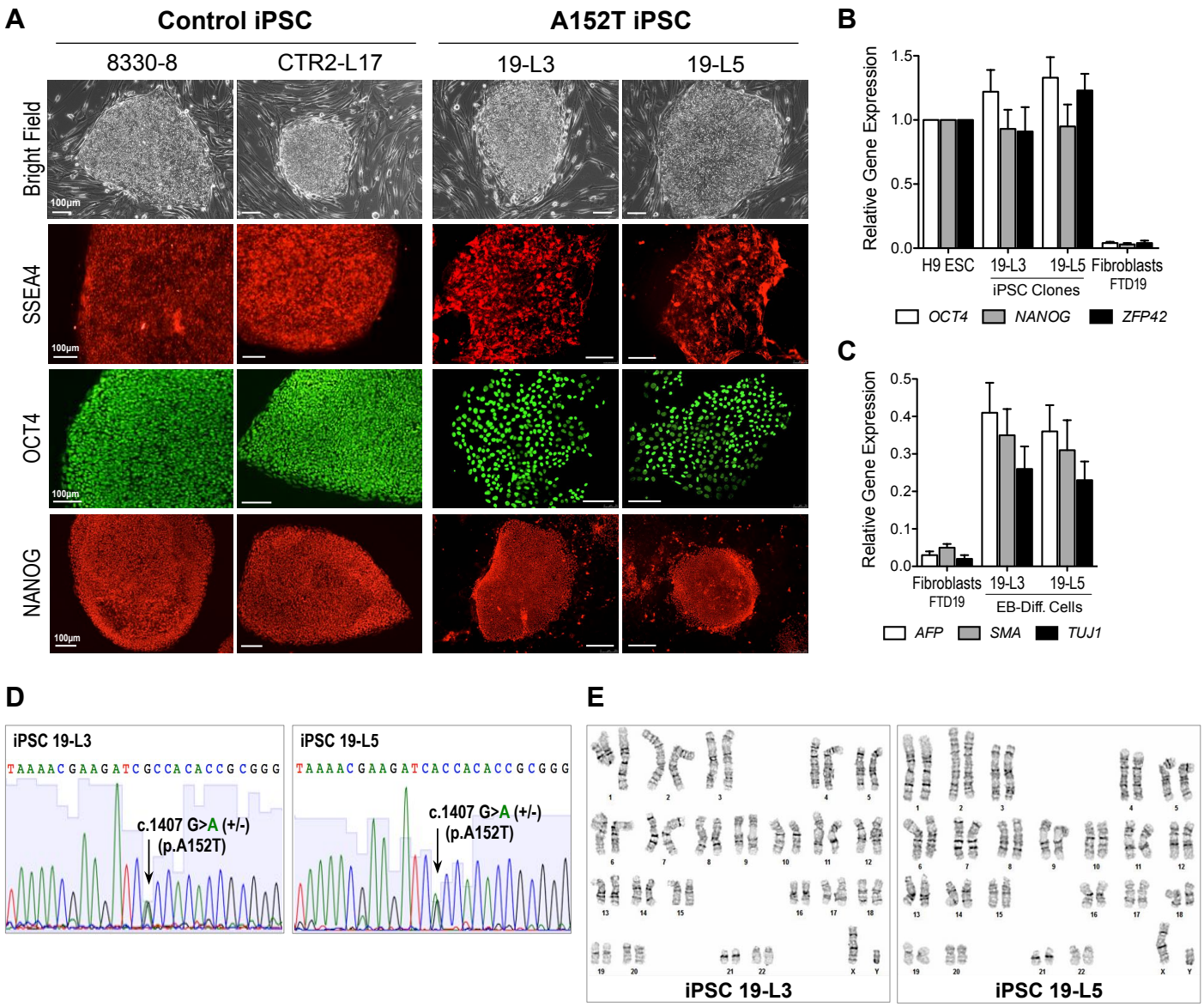

Figure S1. Characterization of iPSC Lines. Related to Figure 1.

(A) Bright-field images of iPSCs, and IF analysis of pluripotency markers SSEA-4, NANOG and OCT4 in Control and A152T iPSC lines. Scale bar 100µm. SSEA4 and OCT4 images for A152T iPSCs were taken immediately after cell passaging before dense colonies formed, it does not represent a phenotype.

(B) Transcript levels (mean ±SD) of pluripotency genes *OCT4*, *NANOG* and *ZFP42* in iPSC 19-L3 and 19-L5, by qRT-PCR (n =3), compared to the human H9-ESC line (positive control) and the original FTD19 fibroblast line (negative control).

(C) Transcript levels (mean ±SD) of endogenous germ layer markers by qRT-PCR (n =3), upon *in vitro* embryoid body differentiation (EB-Diff.) of 19-L3 and 19-L5 iPSCs. Trilineage markers were *TUJ1* (ectoderm), *SMA* (mesoderm) and *AFP* (endoderm). FTD19 fibroblasts served as negative control.

(D) DNA sequencing of the *MAPT* c.1407G>A locus in genomic DNA from iPSC 19-L3 and 19-L5 confirmed the heterozygous missense variant A152T.

(E) G-band karyotype analysis of iPSC clones 19-L3 and 19-L5.

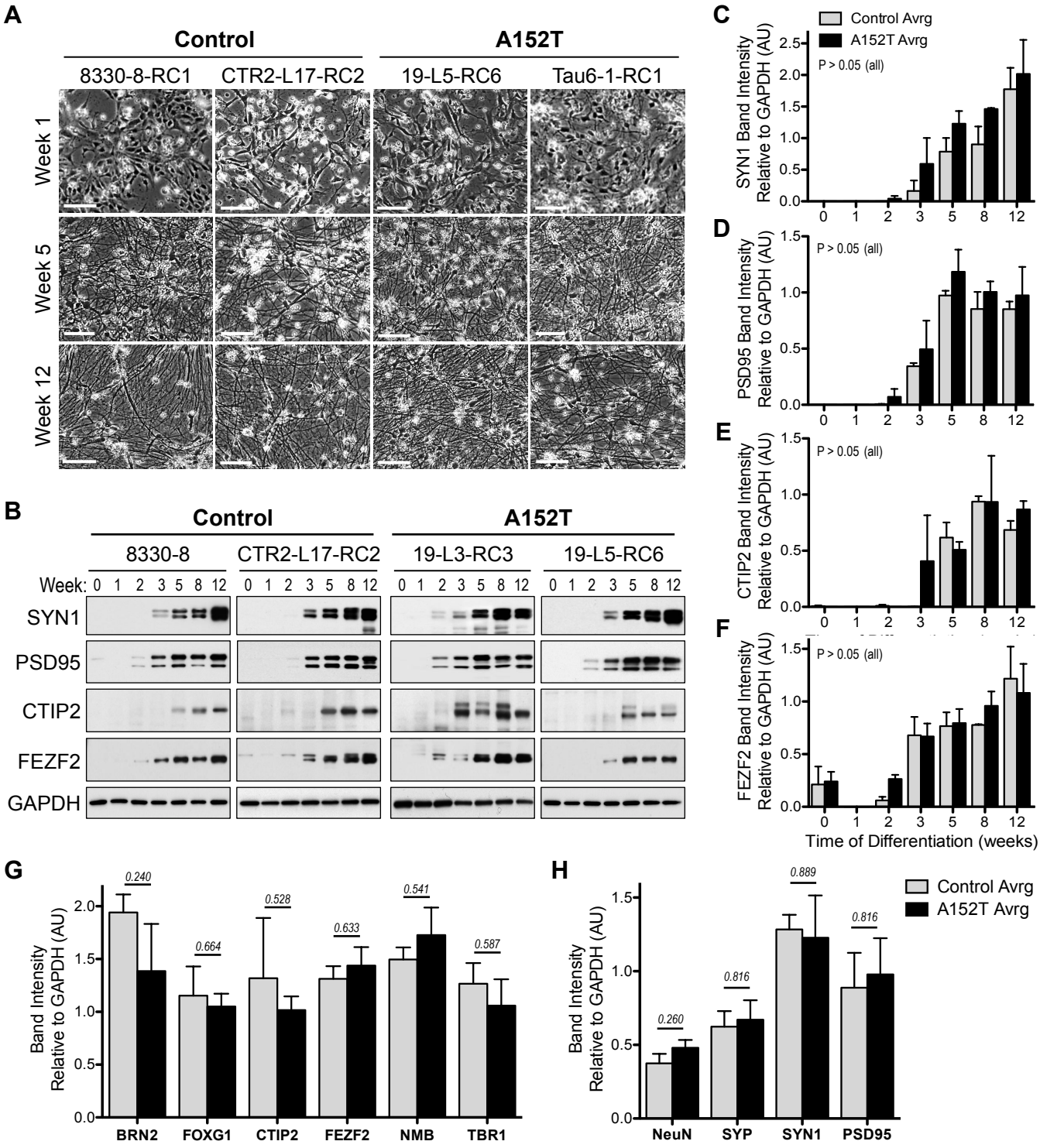

Figure S2. NPC Differentiation Time-Course Assessment. Related to Figure 1.

(A) Bright-field images at 1, 5 and 12 weeks of NPC differentiation, for two Control and two A152T lines. Scale bar 100μm (representative images).

(B) Time-course expression of synaptic (SYN1, PSD95) and cortical layer V (CTIP2, FEZF2) protein markers by Western blot analysis, in neuronal cells up to 12 weeks of differentiation. GAPDH served as loading control.

(**C-F**) Semi-quantitative analysis of Western blots as in (B). Band intensities in arbitrary units (AU), showing averaged (Avrg) values across lines of the same genotype ±SEM; two-way ANOVA and Bonferroni post-test P>0.05, *n*=3 independent experiments.

(**G, H**) Semi-quantitative analysis of Western blots as in Figure 1C (**G**) and Figure 1D (**H**), showing relative levels of cortical and synaptic markers, respectively, in 5-week differentiated neurons. Band intensities in arbitrary units (AU), showing averaged (Avrg) values across lines of the same genotype ±SEM, Student t-test *p*-value shown, *n*=3 independent experiments.

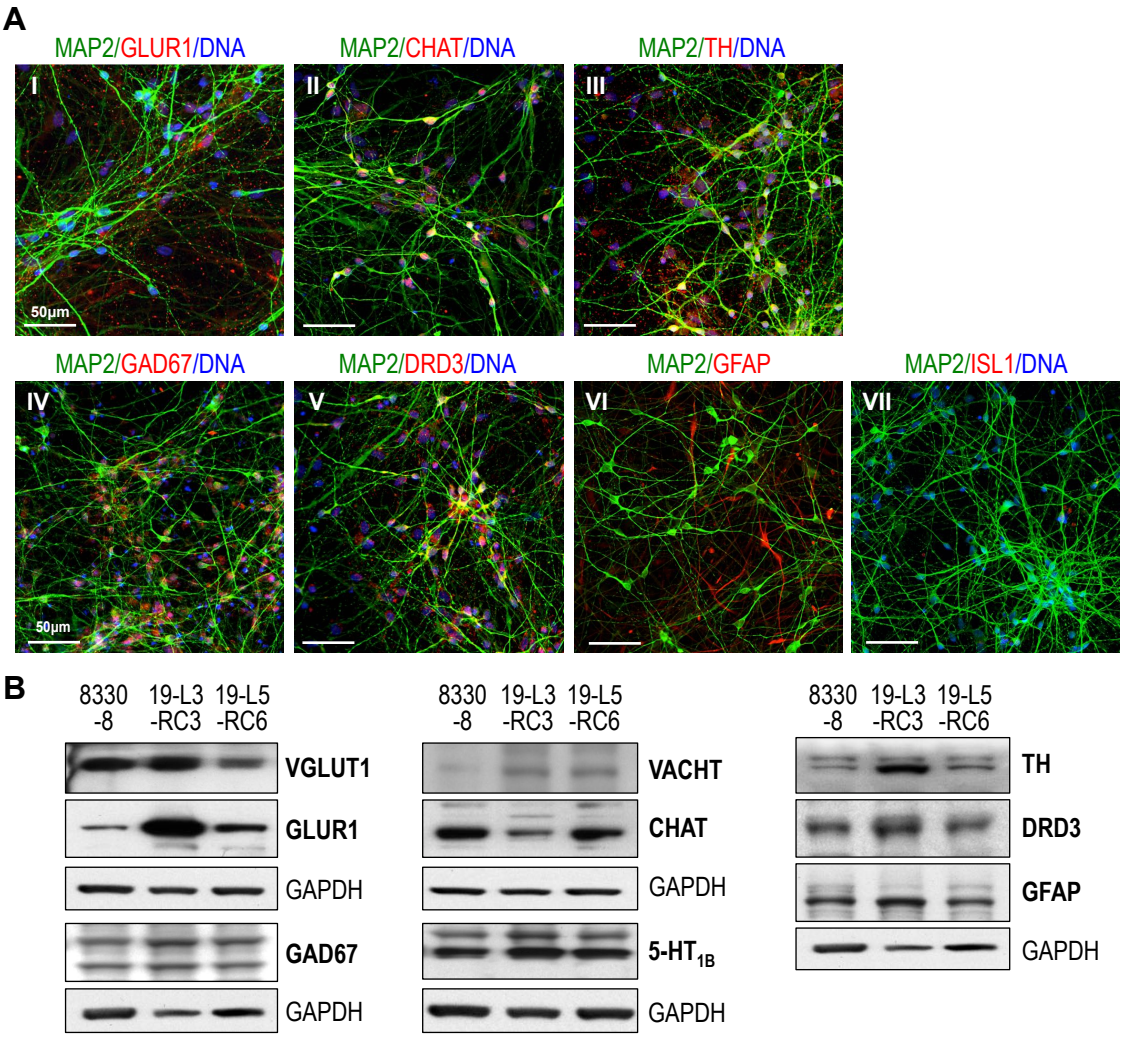

Figure S3. Expression of Neuronal Markers in iPSC-Derived Neurons. Related to Figure 1.

(A) IF analysis of neuronal markers (*red*) in 5-week differentiated neurons, with MAP2 (*green*) and nuclear DNA (*blue*) co-staining. Representative images irrespective of *MAPT* genotype (showing 19-L3-RC3). Scale bar 50µm.

(B) Expression of neuronal markers by Western blot analysis, in Control (8330-8) and A152T (19-L3-RC3, 19-L5-RC6) 5-week differentiated neurons. GAPDH served as loading control.

Markers tested: glutamatergic GLUR1 (glutamate receptor 1, or GRIA) and VGLUT1 (vesicular glutamate transporter 1); cholinergic CHAT (choline acetyltransferase) and VACHT (vesicular acetylcholine transporter); TH (tyrosine hydroxylase); GABAergic GAD67 (glutamate decarboxylase); dopaminergic/adrenergic DRD3 (dopamine receptor D3); glial GFAP (glial fibrillary acidic protein); serotonergic 5-HT_{1B} (5-hydroxytryptamine receptor 1B); and neural crest/cardiomyocyte lineage ISL1 (islet-1).

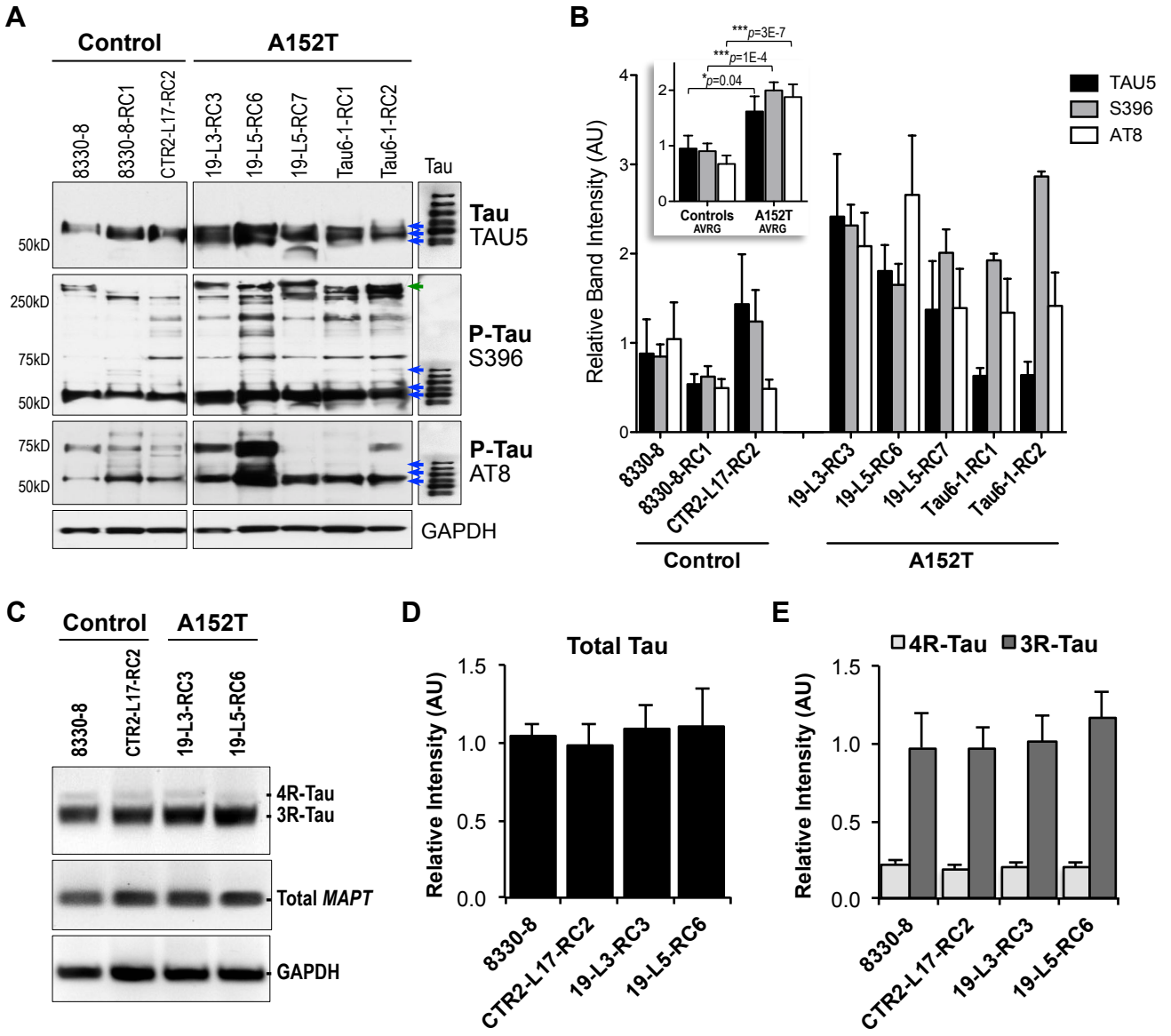

Figure S4. Upregulation of Tau in A152T Neurons, with Constant *MAPT* Gene Expression. Related to Figure 2.

(**A**) Analysis of total tau (TAU5) and P-tau (S396, AT8) levels in Control and A152T neurons (5 weeks), by Western blot. Rightmost panels show recombinant human tau (six isoforms, no PTMs); GAPDH served as loading control. Samples ran in the same blot and cropped for clarity of this figure. Blue arrows (migration within tau-ladder) and green arrows (HMW) correspond to bands quantified in (B).

(**B**) Semi-quantitative analysis of Western blots as in (A). Band intensities (arbitrary units, AU) shown relative to GAPDH (mean ±SEM). Inset graph shows averaged values for all Control lines vs. all A152T lines, for each antibody. Student t-test *p*-value in shown, n≥3 independent experiments.

(C) Endogenous *MAPT* transcript levels by RT-PCR analysis of 5-week differentiated neurons. Assessment of total *MAPT* expression and 3R/4R-tau isoforms resulting from alternative splicing of exon 10. *GAPDH* served as loading control; representative gel from *n*=3 independent experiments.

(D-E) Semi-quantitative analysis of total-*MAPT* (**D**) and 3R-tau, 4R-tau (**C**) transcripts' band intensities shown in (C), relative to *GAPDH* (mean arbitrary units ±SEM; *n*=3 independent experiments).

A

A152T tau
ITTPRGAAPPGQK

Residue	b	b+2	y	y+2
I	114.0913	57.5493	1293.7274	647.3673
T	**215.1390**	108.0731	1180.6433	**590.8253**
T	316.1867	158.5970	1079.5956	**540.3014**
P	413.2395	207.1234	**978.5479**	**489.7776**
R	569.3406	285.1739	881.4952	441.2512
G	626.3620	313.6847	**725.3941**	363.2007
A	697.3991	349.2032	668.3726	334.6899
A	**768.4363**	384.7218	597.3355	299.1714
P	865.4890	433.2482	**526.2984**	**263.6528**
P	**962.5418**	481.7745	**429.2456**	**215.1264**
G	1019.5633	**510.2853**	**332.1928**	166.6001
Q	1147.6218	574.3146	**275.1714**	138.0893
K	1275.7168	638.3620	147.1128	74.0600

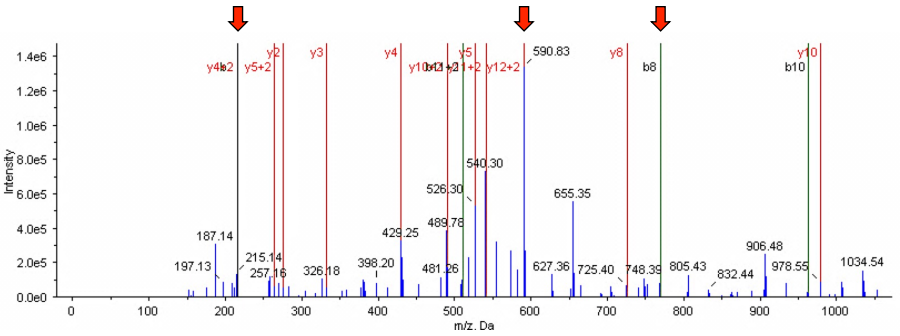

B

Non-mutant tau
IATPRGAAPPGQK

Residue	b	b+2	y	y+2
I	114.0913	57.5493	1263.7168	632.3620
A	**185.1285**	93.0679	1150.6327	**575.8200**
T	286.1761	143.5917	1079.5956	**540.3014**
P	383.2289	192.1181	**978.5479**	**489.7776**
R	539.3300	270.1686	881.4952	441.2512
G	596.3515	298.6794	**725.3941**	363.2007
A	**667.3886**	334.1979	668.3726	334.6899
A	**738.4257**	369.7165	597.3355	299.1714
P	835.4785	418.2429	**526.2984**	**263.6528**
P	932.5312	466.7693	**429.2456**	215.1264
G	989.5527	495.2800	**332.1928**	166.6001
Q	1117.6113	559.3093	275.1714	138.0893
K	1245.7062	623.3568	147.1128	74.0600

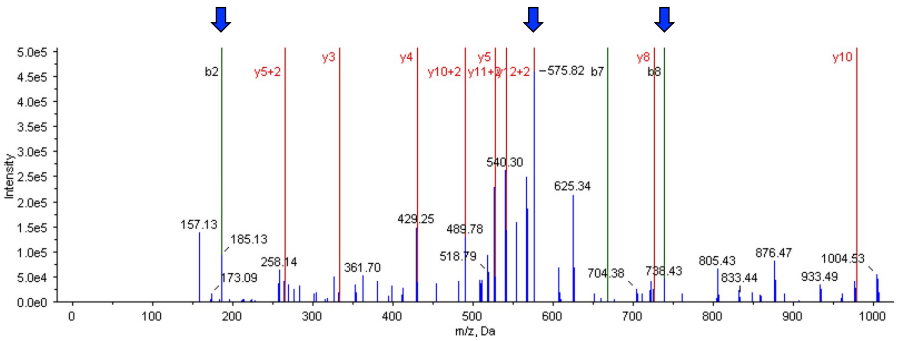

Figure S5. MS Spectral Evidence of Non-Mutant and A152T Tau Peptides in FTD Neurons. Related to Figure 4.

A152T neurons (8-week differentiated) were subjected to LysC digestion and the peptide mixture was analyzed by shotgun MS. Shown are exemplary lists of detected product ions and the corresponding fragmentation spectrum for **(A)** the tau-A152T peptide 'ITTPRGAAPPGQK' and **(B)** the non-mutant tau peptide 'IATPRGAAPPGQK'. Distinguishing product ion species are highlighted in red and blue, respectively.

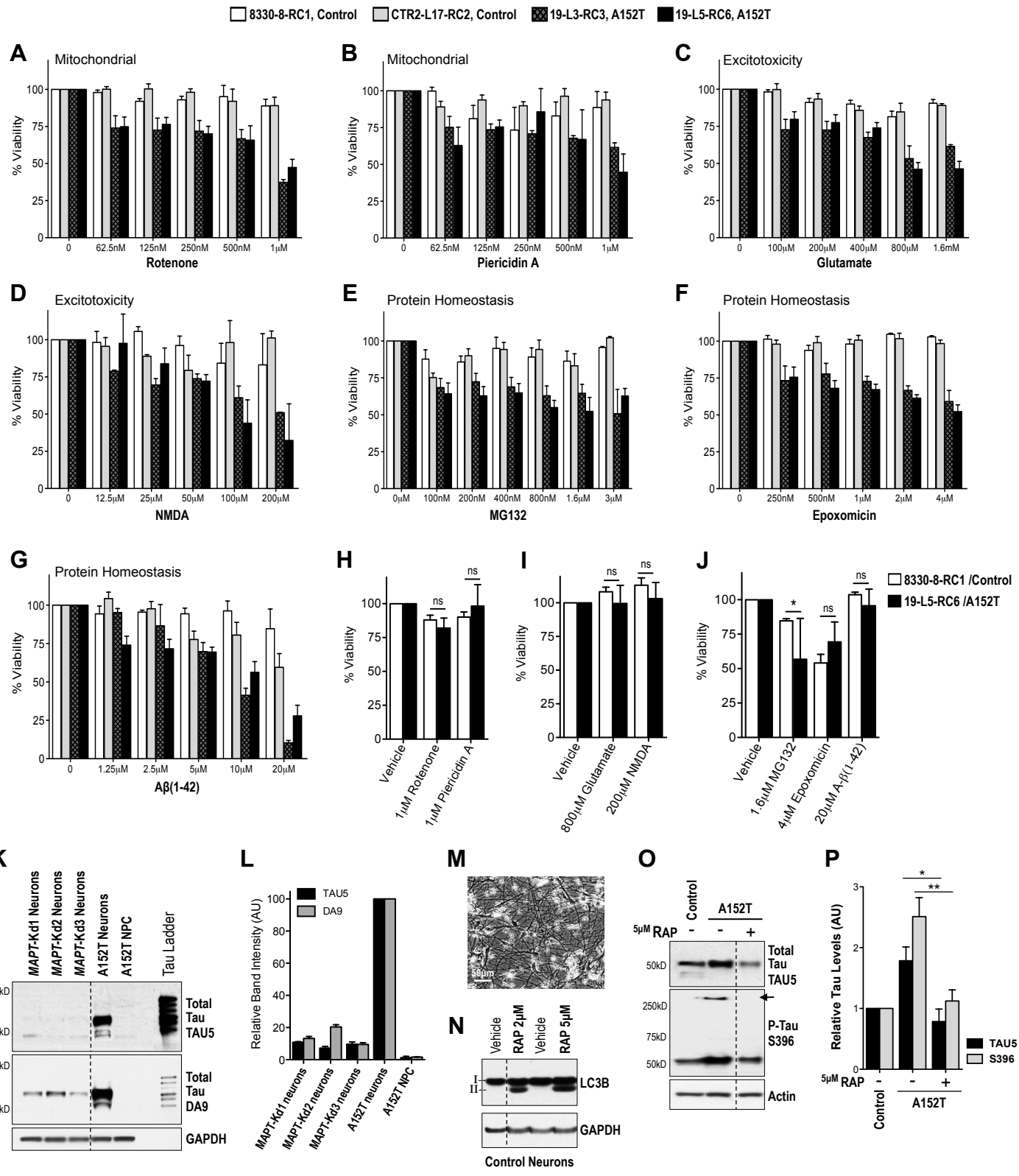
8330-8-RC1, Control
CTR2-L17-RC2, Control
19-L3-RC3, A152T
19-L5-RC6, A152T
A
Mitochondrial
% Viability
Rotenone
B
Mitochondrial
Piericidin A
C
Excitotoxicity
Glutamate
D
Excitotoxicity
NMDA
E
Protein Homeostasis
MG132
F
Protein Homeostasis
Epoxomicin
G
Protein Homeostasis
Aβ(1-42)
H
Vehicle
1μM Rotenone
1μM Piericidin A
I
Vehicle
800μM Glutamate
200μM NMDA
J
8330-8-RC1 /Control
19-L5-RC6 /A152T
Vehicle
1.6μM MG132
4μM Epoxomicin
20μM A-β(1-42)
K
MAPT-Kd1 Neurons
MAPT-Kd2 Neurons
MAPT-Kd3 Neurons
A152T Neurons
A152T NPC
Tau Ladder
Total Tau TAU5
Total Tau DA9
GAPDH
L
TAU5
DA9
Relative Band Intensity (AU)
M
50μm
N
Vehicle
RAP 2μM
Vehicle
RAP 5μM
LC3B
GAPDH
Control Neurons
O
Control
A152T
5μM RAP
Total Tau TAU5
P-Tau S396
Actin
P
Relative Tau Levels (AU)
TAU5
S396
5μM RAP
Control
A152T

Figure S6. Chemical Stressors Effect on Cell Viability and Rescue by Tau Down-Regulation. Related to Figure 7.
(**A-G**) Dose-dependent cell viability of Control and A152T 8-week differentiated neurons, after 24h treatment. Mean values are shown as % viability of vehicle-treated neurons (±SEM, n=3 independent experiments).
(**H**-**J**) Cell viability of Control and A152T 2-week differentiated neural cells, after 24h treatment. Mean values are shown as % of vehicle-treated cells (±SEM, two-way ANOVA and Bonferroni post-test non-significant/ns P>0.05, *P<0.05, n=3 independent experiments).
(**K-M**) CRISPR/Cas9-mediated genetic knockdown of *MAPT* expression in three independent cell lines, derived from the 19-L5-RC6 A152T line: *MAPT*-kd1, *MAPT*-kd2, *MAPT*-kd3. (**K**) Western blot levels of tau (TAU5 and DA9 antibodies) in 4-week differentiated neurons, relative to the original cell line (19-L5-RC6, A152T neurons) and the correspondent A152T NPCs as positive control for no tau protein expression. (**L**) Semi-quantitative analysis of (K), band intensities are relative to GAPDH in arbitrary units (AU) and normalized to the original cell line (19-L5-RC6) A152T neurons as 100% (mean ±SD, n =3 independent experiments). (**M**) Phase image of *MAPT*-kd3 neurons upon 8 weeks of differentiation without morphological alterations relative to the original line (scale bar 50μm).
(**N**) Western blot analysis of 5-week differentiated neurons (Control 8330-8-RC1) upon 24h treatment with rapamycin (RAP, 2μM or 5μM) shows activation of autophagy (LC3B-II, lower band). Samples ran in the same blot and cropped for the purpose of this figure *only* (n >3 independent experiments).
(**O, P**) Western blot analysis of total tau (TAU5) and P-tau (S396) in 5-week differentiated neurons treated with 5μM rapamycin for 24h (+), in comparison with vehicle-treated (-) neurons (Control 8330-8-RC1 and 19-L5-RC6 A152T line), showing downregulation of tau by RAP (including down-regulation of the HMW-tau, *arrow*). Actin was used as loading control. Samples ran in the same blot and cropped for the purpose of this figure only. (**P**) Semi-quantitative analysis of (O). Band intensities are relative to Actin in arbitrary units (AU), normalized to vehicle-treated Control as 100% (mean ±SEM, n >3 independent experiments). Student t-test *p<0.05, **p<0.01.

Supplemental Table

Table S1. Human-Derived iPSC and NPC lines. Related to Figure 1 and Figure 2.

Donor (age)	*MAPT*	Fibroblast	iPSC Lines	NPC Lines
Male (63) unaffected	non-mutant (+/+)	GM08330	8330-8 [(1)]	8330-8 8330-8-RC1
Male (52) unaffected	non-mutant (+/+)	CTR2-17	CTR2-L17 [(3)]	CTR2-L17-RC2
Male (65) PSP	A152T (-/+) rs143624519	FTD19	19-L3 [(3)] 19-L5	19-L3-RC3 19-L5-RC6 19-L5-RC7
Male (75) asymptomatic	A152T (-/+) rs143624519	Tau6	Tau6-1[(2)]	Tau6-1-RC1 Tau6-1-RC2

[(1)]Sheridan S.D., *et al*. 2011; [(2)]Fong H., *et al*. 2013; [(3)]Biswas H.U., Gao F.B., *personal communication*.

Supplemental Experimental Procedures

Antibodies Used in This Study and Respective Commercial Information
Human iPSC and NPC markers: SSEA4 (stage-specific embryonic antigen-4, surface marker) Stemgent StainAlive 09-0097; NANOG (Homeobox Transcription Factor Nanog) Abcam ab21624; OCT4 (Octamer-binding transcription factor 4) Santa Cruz Biotech sc-5279; Nestin (neural type VI intermediate filament protein) Millipore AB5922; SOX2 (transcription factor SRY-box 2) Abcam ab59776; PAX6 (embryonic transcription factor paired box protein) Developmental Studies Hybridoma Bank (3/29/2012); Musashi-1 (NPC RNA-binding protein) Millipore AB5977. **Total tau antibodies:** TAU1 (non-P-S199/S202/T205) Millipore MAB3420; TAU5 (aa210-aa241) Invitrogen AHB0042; DA9 (aa102-aa140) kindly provided by Dr. Peter Davies; K9JA (MTBD) DAKO A0024. **Phospho-tau antibodies:** AT8 (tau-pS202/S205) Thermo MN1020; AT180 (tau-pT231/pS235) Thermo MN1040; S396 (tau-pS396) Invitrogen 44752G; PHF-1 (tau-pS396/pS404) kindly provided by Dr. Peter Davies. **Neuronal markers:** NeuN (neuronal RNA-binding protein, nuclear) Abcam ab104225; MAP2 (microtubule-associated protein 2) Chemicon AB5543; TBR1 (T-box, brain, 1 transcription factor, neuronal migration) Abcam ab31940; CTIP2 (zinc-finger transcription repressor, subcortical projecting neurons) Abcam ab18465; FEZF2 (ZNF312/ zinc-finger protein 2 transcription repressor, subcortical neurons) Santa Cruz sc-100259; FOXG1 (Forkhead box-G1 transcription repressor) Abcam ab18259; BRN2 (POU3F2/ POU domain, class 3, transcription factor 2) Santa Cruz Biotech sc-6029; NMB (neuromedin B) VWR PIPA525267/Thermo PA5-25267; SYP (synaptophysin, major synaptic vesicle protein p38) Sigma S-5768; SYN1 (synaptic protein Synapsin I) Synaptic Systems 106103; PSD95 (post-synaptic density protein 95) Neuro-Mab 75-028; VGLUT1 (vesicular glutamate transporter 1) Synaptic systems 135 304; GLUR1 (glutamate receptor 1/GRIA1) Millipore AB1504; GAD67 (glutamate decarboxylase) Millipore AB1511; VACHT (vesicular acetylcholine transporter) Millipore AB1588; CHAT (cholinergic acetyltransferase) Millipore AB143; DRD3 (Dopamine Receptor D3) Abcam ab42114; TH (tyrosine hydroxylase) Sigma T2928; GFAP (glial fibrillary acidic protein, intermediate filament) EnCor MCA-5C10; 5HT1B (serotonin receptor) Abcam ab13896; ISL1 (anti-Islet 1) Abcam ab109517. **Autophagy Markers and Chaperones:** LC3B (autophagy marker Light Chain 3/LC3B I and II) Cell Signaling Tech 3868; LAMP1 (lysosome-associated membrane protein 1) Abcam ab25630; LAMP2a (lysosome-associated membrane protein 2a) Abcam ab18528; SQSTM1(p62/sequestosome 1, ubiquitin binding protein, autophagy substrate) Enzo Lifesciences BML-PW9860; ATG12 (Autophagosome marker, ATG12 and ATG12-ATG5 complex) Cell Signaling Tech 2010; HSP70 (heat shock protein 70kDa) Enzo Life Sciences ADI-SPA-810-D; CHIP (co-chaperone, carboxy terminus of Hsc70-interacting protein) Cell Signaling Tech 2080; HSP90 (heat shock protein 90kDa) Cell Signaling Tech 4877; UBI-1 (ubiquitin) Millipore MAB1510; HOP (STIP, HSP70/HSP90 co-chaperone stress-induced phospho protein 1) Cell Signaling Tech 5669; HIP (HSP70-interacting protein, HSP70 co-chaperone) Cell Signaling Tech 2723. **ER-UPR:** PERK-pThr980 (phosphorylated protein kinase-like endoplasmic reticulum kinase) Cell Signaling Tech 3179S; PERK (protein kinase-like endoplasmic reticulum kinase) Santa Cruz sc-9479; eIF2α-pSer51 (phosphorylated eukaryotic initiation factor 2, α subunit) Abcam ab32157; eIF2α (eukaryotic initiation factor 2, α subunit) Cell Signaling Tech 5324P; IRE1α-pSer724 (phosphorylated ER Ser/Thr-protein kinase/ endoribonuclease) Novus Biologicals NB100-2323; IRE1α (ER serine/threonine-protein kinase/ endoribonuclease) Cell Signaling Tech 3294P; BiP (GRP78 / ER-heat shock protein 78kDa) Cell Signaling Tech 3177P; CHOP (C/EBP-homologous protein inhibitor of C/EBP,LAP DNA binding) Thermo MA 1-250. **Internal Controls:** GAPDH (glyceraldehyde 3-phosphate dehydrogenase) Abcam ab8245; Actin (β-Actin) Sigma A1978.

Reprograming of Human Dermal Fibroblasts
Skin biopsy-derived human fibroblasts were grown in flasks with filter-sterilized fibroblast medium: 10% heat-inactivated FBS (Gemini Bio-Products), 1% penicillin-streptomycin (Gibco), 1% L-glutamine (Gibco) and 88% DMEM (Gibco). iPSCs were generated by retroviral reprogramming as previously described [Biswas, Gao *et al*., personal communication; (Fong et al., 2013; Takahashi et al., 2007; Takahashi and Yamanaka, 2006)]. Briefly, fibroblasts were infected with retroviral vectors expressing the four transcription factors OCT4, SOX2, KLF4, and c-MYC, and then plated onto gelatin-coated dishes with γ-irradiated mouse embryonic fibroblasts (iMEFs/ GlobalStem), and filter-sterilized iPSC culture medium [20% Knock-Out Serum Replacement (KOSR/ Gibco), 1 mM L-glutamine (Gibco), 1% non-essential amino acids (Gibco), 1% penicillin-streptomycin (Gibco), 100 mM 2-mercaptoethanol (BioRad) and 77.5% DMEM/F-12 (Gibco) supplemented with 10 ng/mL bFGF (Stemgent)]. iPSC colonies were first assessed based on morphology and were mechanically isolated and clonally expanded with daily iPSC medium changes, and cryopreserved. RT-PCR analysis of the iPSC clones with primers specific for the transgenes *OCT4/POU5F1*, *SOX2*, *KLF4*, and *c-MYC*, confirmed complete transgene silencing (not shown). Cells were passaged manually or detached by incubation with Accutase (Sigma). For downstream analysis and derivation, iPSC colonies were manually transferred onto matrigel-coated (BD Biosciences) plates with mTeSR1 medium (Stem Cell Technology) supplemented with 1% penicillin-

streptomycin (Gibco). Feeder-free iPSCs were further expanded with daily media changes, passaged by brief incubation with 1 mg/mL Dispase (StemCell Technologies), and cryopreserved. Nomenclature of each iPSC line reflects the original fibroblast cell line name, plus a number (L#) indicative of the colony it was derived from (Table S1).

Characterization of iPSC Lines

For IF analysis of pluripotency markers, iPSC colonies grown on iMEFs-coated 24-well plates were fixed in 4% (v/v) formaldehyde-PBS (Tousimis, Corning) for 15 min at room temperature, permeabilized in 0.2% (v/v) Triton X-100/PBS (Biorad) for 30 min, and blocked in 3% (w/v) BSA/PBS (Sigma) for 2h at room-temperature. Cells were incubated overnight at 4°C with the primary antibodies, followed by the corresponding AlexaFluor conjugated secondary antibodies (Life Technologies). Images were acquired using a Zeiss Axiovert inverted microscope equipped with a Zeiss Axiocam digital camera. Characterization of these iPSC lines has also been shown elsewhere [Biswas, Gao *et al*., personal communication; (Almeida et al., 2012; Fong et al., 2013)].

DNA Sequencing

Genomic DNA was isolated from FTD19-derived iPSC clones with GenElute Mammalian Genomic DNA Miniprep Kit (Sigma), following manufacturer's instructions. Genomic DNA (250 ng) was PCR-amplified using Phusion High Fidelity DNA Polymerase (Thermo) with 0.5 μM forward and reverse primers flanking the A152T locus on the *MAPT* gene, to yield a 347-bp fragment. Forward and reverse primer sequences were as follows: Forward 5'-TCAGGGAACTTGGAGTTTGG-3' and Reverse 5'-TTCTTACCAGAGCTGGGTGG-3'. The A152T variant and non-mutant *MAPT* alleles were also confirmed in the other clones by DNA sequencing [Biswas, Gao *et al*., personal communication, (Fong et al., 2013), and not shown].

RNA Extraction and RT-PCR Analysis

Cells were collected in PBS and pelleted at 3,000*g* for 5 min. Total RNA extraction was performed using the RNeasy Plus Mini Kit (Qiagen Cat.74134), according to the manufacturer's instructions with an added step of in-column DNase I digestion, before RNA elution. RNA was quantified by Nanodrop, and reverse transcribed using the iScript cDNA Synthesis Kit (Bio-Rad Cat.170-8891). Standard PCR was performed with Phusion Green Hot Start II High-Fidelity DNA Polymerase (Thermo) and samples were run on a 1% (w/v) Agarose-TAE buffer gel. For semi-quantitative analysis (Figure S4C-E), gels were scanned using the AlphaImager System 2200 (Alpha Innotech, Genetic Technologies), and band intensities (pixel mean intensity) were quantified using Adobe Photoshop CS5 Histogram function. Relative intensity was calculated relative to the respective control GAPDH band.

Primers were as follows for *MAPT* isoforms *3R+4R* Fw 5′-CCCAGCTCTGGTGAACCTCCA-3′, Rev 5′-TCACAAACCCTGCTTGGCCAG-3′; for total *MAPT* Fw 5'-CAAGCTCGCATGGTCAGTAA-3', Rev 5'-CAGAGCTGGGTGGTGTCTTT-3'; and for *GAPDH* Fw 5'-CCATGGCACCGTCAAGGCTGA-3', Rev 5′-GCCAGTAGAGGCAGGGATGAT-3′. Primers for endogenous pluripotency-associated genes were: *OCT4* Fw 5'-GTACTCCTCGGTCCCTTTCC-3', Rev 5'-CAAAAACCCTGGCACAAACT-3'; *NANOG* Fw 5'-CAAAGGCAAACAACCCACTT-3', Rev 5'-TCTGCTGGAGGCTGAGGTAT-3'.

***In vitro* Differentiation of Embryoid Bodies and Tri-Lineage Analysis**

For spontaneous differentiation, iPSC colonies were detached with Accutase (Millipore) and grown as embryoid bodies (EBs) in suspension for 8 days in iPSC medium without basic fibroblast growth factor (bFGF). EBs were then allowed to adhere to Matrigel-coated plates and further differentiate for 8 days in mTeSR1 medium. Cells migrating out of the attached EBs were collected for RNA extraction and analysis of markers of the three germ layers: β-III tubulin (*TUJ1*) for ectoderm, smooth muscle actin (SMA) for mesoderm, and alpha-fetoprotein (AFP) for endoderm. Primers for the trilineage markers were: *AFP* Fw 5'-TGTACTGCAGAGATAAGTTTAGCTGAC-3', Rev 5'-TCCTTGTAAGTGGCTTCTTGAAC-3'; *SMA* Fw 5'-TTCAATGTCCCAGCCATGTA-3', Rev 5-GAAGGAATAGCCACGCTCAG-3'; *TUJ1* Fw 5'-GCAACTACGTGGGCGACT-3', Rev 5'-CGAGGCACGTACTTGTGAGA-3'.

Derivation of NPC Lines and Flow Cytometry Cell Sorting

Expandable iPSC-derived NPCs, for the three A152T iPSC clones (19-L3, 19-L5, Tau6-1) and additional Control lines (8330-8, CTR2-L17) were generated using STEMdiff Neural Induction medium and the Aggrewell Plate 800 microwells (StemCell Technologies) method of embryoid bodies (EBs) formation according to manufacturer's instructions (Koch et al., 2009; Nemati et al., 2011; Ungrin et al., 2008). Briefly, iPSCs were detached with Accutase (Sigma), pelleted at 300*g* for 5 min and resuspended in NIM (STEMdiff Neural Induction Media, StemCell Technologies) supplemented with ROCK inhibitor Y-27632 at 10 μM (InSolution EMD Biosciences). On average, $2.5x10^6$ cells were plated per aggrewell in NIM/Y-27632, and allowed to form

EBs for 5 days, with daily medium change. EBs were transferred to poly-ornithine (20 μg/mL in water, Sigma) and laminin (5 μg/mL in PBS, Sigma) /POL-coated plates and cultured in NIM for another 5-7 days, with daily media changes. At this point, EBs showed the formation of 3-dimentional neural rosette clusters that were manually detached with an angle fire-polished Pasteur pipette, under a microscope, and transferred to new POL/NIM plates for 2 days. Then, medium was switched to DMEM/F12-B27 (70% DMEM/ Gibco, 30% Ham's-F12/ MediaTech, 2% B27/ Gibco, 1% penicillin-streptomycin/ Gibco) supplemented with EGF (20 ng/mL, Sigma), FGF (20 ng/mL, Stemgent) and heparin (5 μg/mL, Sigma), to promote proliferation. Media changes were performed every other day or as needed, and after approximately 6 days in culture, cells were subjected to flow cytometry sorting (FACSed/ fluorescence-activated cell sorting), for $CD184^{+}$/ $CD133^{+}$/ $CD271^{-}$ cells, with the goal of enriching the generated NPC lines towards neural cortical-like progenitors (Yuan et al., 2011).

For flow cytometry, neural rosettes were detached with TrypLE (Life Technologies), filter-strained to disassemble the clusters, and resuspended in FACS buffer [2% (v/v) B27 (Gibco); 20 mM glucose (Sigma), 1% (v/v) penicillin-streptomycin (Gibco), 1 mM EDTA (Sigma), 92.8% (v/v) HBSS (Gibco, w/o Ca^{2+}/Mg^{2+}/phenol-red, 10 ng/mL bFGF (StemGent), filter-sterilized]. Cell suspension was incubated with DNase I (DNase I 1 U/μL, 10 min), followed by 5% (w/v) BSA-water (Sigma), and finally the cell surface markers: PE-CD133 (Miltenyi Biotec Cat. 130-080-801), APC-CD184 (BD Pharmigen Cat. 555976), PerCP-Cy5.5-CD271 (BD Pharmigen Cat. 560 834) and DAPI, for 20 min at 4°C. Cells were sorted in the BD FACS-ARIA II flow cytometer (BD Biosciences) with a 100 μm nozzle and 20 psi sheath pressure, collected onto eppendorf tubes containing DMEM/F12-B27 with EGF/FGF/heparin (E.F.H.) medium, and plated in POL plates. Cells were passaged every 3-4 days with TrypLE and kept on POL plates and DMEM/F12-B27 media. Nomenclature of each NPC line reflects the original iPSC name, plus a number indicative of the rosette-clusters that it derived from (-RC#, Table S1).

For neural progenitor lineage assessment by IF, cells were plated onto POL-coated coverslips (Chemglass Lifesciences) in 24-well plates, with expansion medium, until they reached 70-80% confluency. NPCs were fixed in 4% (v/v) formaldehyde-PBS (Tousimis, Corning), incubated with 1% (v/v) FBS (Gemini Bio-Products) and 0.1% (v/v) Triton X-100 (Biorad) in PBS for 2h, followed by primary antibody NESTIN, SOX2, Musashi and PAX6 incubation, and subsequent AlexaFluor-conjugated secondary antibodies (Life Technologies). The glass coverslips were mounted onto ProLong Gold Antifade Reagent (Life Technologies) glass slides for microscopy analysis (Zeiss Axiovert).

To ensure genomic stability in NPCs kept in culture over 30 passages, we performed array-based comparative genomic hybridization (aCGH) analysis (Cell Line Genetics, Inc.) to detect any structural, deletions or insertions chromosomal alterations, *i.e.* sub-karyotype anomalies that could potentially affect disease-relevant phenotypes (Elliott et al., 2010; Villa-Diaz et al., 2014). No chromosomal aberrations >5Mb were detected in any of the NPC lines.

Karyotype and aCGH Analysis

For G-band karyotype analysis, each iPSC line (live cultures on Matrigel matrix) was karyotyped by Cell Line Genetics or as previously described [Biswas, Gao *et al*., personal communication; (Almeida et al., 2012; Fong et al., 2013; Sheridan et al., 2011)]. For array Comparative Genomic Hybridization (aCGH) analysis, frozen cell pellets of each of the six NPC lines (proliferative state) were sent to Cell Line Genetics for DNA extraction, QC and analysis of unbalanced structural and numerical chromosomal alterations (SurePrint G3 Human CGH Microarray Kit; with average coverage every 41KB with increased coverage in RefSeq genes). List of genes found with amplifications or deletions is available upon request.

NPC Differentiation and IF Analysis

NPCs were plated and differentiated in 24-well plates POL-coated coverslips (Chemglass Lifesciences), or in 96-well black clear-bottom plates (Corning 3904). Neurons were fixed in 4% (v/v) formaldehyde-PBS (Tousimis) for 20 min, washed in PBS (Corning), incubated in blocking/permeabilization buffer [10 mg/mL BSA (Sigma), 0.05% (v/v) Tween-20 (Biorad), 2% (v/v) goat serum, 0.1% Triton X-100 (Biorad), 92% (v/v) PBS] for 2h at room temperature, followed by overnight incubation with primary antibodies (above), and then incubated with the corresponding AlexaFluor conjugated secondary antibodies (Life Technologies). Glass coverslips-cultured neurons were mounted onto ProLong Gold Antifade Reagent (Life Technologies) slides, whereas neurons cultured in 96-well plates were imaged directly from the plates. Image acquisition was done with the IN Cell Analyzer 6000 Cell Imaging System (GE Healthcare Life Sciences).

Protein Analysis by Western Blot

Neurons were washed and collected in PBS, lysed in RIPA buffer (Boston Bio-Products) with 2% SDS (Sigma), protease inhibitors (Roche Complete Mini tablets), and phosphatase inhibitors (Sigma), followed by sonication

in a water sonicator (Bransonic Ultrasonic Baths, Thomas Scientific) for 5 min, and centrifugation at 20,000*g* for 15 min. Supernatants were transferred to new tubes and total protein concentration was quantified with the Pierce BCA Protein Assay Kit (Thermo). For human brain sample, a tissue punch from the human anterior cingulate cortex (ACC) was directly lysed in 100 µL of 3X SDS-DTT Blue Loading Buffer with DTT (NEB) and boiled for 10 min. Human recombinant tau protein ladder was purchased from Sigma. Western blots were performed with the Novex NuPAGE SDS-PAGE Gel System (Invitrogen), by running 10 µg of total protein (pre-boiled for 10 min in SDS-DTT loading buffer, NEB) on pre-cast SDS-PAGE. Gels were transferred onto PVDF membranes (EMD Millipore) using standard procedures. Membranes were blocked in 5% nonfat milk in Tris-buffered saline with Tween-20 (TBST/ Biorad) for 2.5 h, incubated overnight with the primary antibodies at 4°C (above), followed by corresponding HRP-linked secondary antibodies (Cell Signaling Technology), and lastly incubated with SuperSignal West Pico Chemiluminescent Substrate (Thermo) according to manufacturer's instructions. Membranes were then exposed to autoradiographic film (LabScientific) for different amounts of time, to account for bands of different intensities (and to ensure detection of all relevant bands). Films were scanned using a GS-800 Calibrated Densitometer (Biorad), and band intensities (pixel mean intensity) were quantified using Adobe Photoshop CS5 Histogram function (bands within tau-ladder migration or otherwise indicated by arrows, including different exposures). Relative intensity was calculated relative to the respective control GAPDH band. For the detection of oxidized proteins, the OxyBlot Protein Oxidation Detection Kit (EMD Millipore) was used according to manufacturer's instructions (Zheng and Bizzozero, 2010).

Expression and Purification of Heavy FLEXITau Standard

Absolute abundance of endogenous tau in neuronal samples was determined using the FLEX peptide light-to heavy (L/H) ratio (Mair et al., 2016; Singh et al., 2009). Heavy isotope labeled tau protein standard was prepared as described previously (Mair et al., 2016). Briefly, tau protein was transcribed and translated from the FLEX vector using the cell-free wheat germ expression (WGE) system according to manufacturer's instructions (Cell Free Sciences, Wheat Germ Expression H Kit-NA). Expression was carried out in the presence of isotope labeled Lysine K8 (13C6 15N2), Arginine R10 (13C6 15N4) and Aspartate D5 (13C4 15N1). The expressed protein was batch-purified using Ni-Sepharose beads (Ni-Sepharose High Performance resin, GE Healthcare), aliquoted and stored at -20°C until use.

FLEXITau Sample Preparation for MS and Analysis

Neuronal cell pellets were resuspended in RIPA buffer as described for western blot. Lysis was performed using Precellys homogenization, followed by centrifugation at 14,000*g* for 30 min. Supernatants were transferred to new tubes, and total protein concentration was determined with the Pierce BCA Protein Assay Kit (Thermo). For FLEXITau experiments, the heavy tau standard was first dephosphorylated by incubation with lambda protein phosphatase (NEB) for 30 min at 30°C and 300rpm. Digestion was performed using 50 to 100 µg of protein lysate or 50 μl dephosphorylated heavy tau standard. Samples were reduced with 50 mM DTT (20 min, 56°C), alkylated with 1% acrylamide (30 min, RT), diluted with 8 M urea and digested using FASP (FASP Protein Digestion Kit, Expedeon) (Wisniewski et al., 2009). Samples were digested overnight at 37°C with 12.5 ng/µl trypsin (Promega) in 50 mM ammonium bicarbonate (ABC), or with 20 ng/µl LysC (Roche) in LysC buffer (0.1 M Tris, pH 9.2, 1 mM EDTA). Peptides were eluted from the membrane two times by 50 mM ABC or LysC buffer and 0.5 M NaCl. Peptides were acidified and desalted using C18 extraction plates (Waters). Vacuum-dried peptides were reconstituted in sample buffer (5% formic acid, 5% acetonitrile) containing the following synthetic peptides *1)* indexed retention time (iRT) peptides (Biognosys); *2)* 50 fmol/μl non-labeled FLEX-peptide TENLYFQGDISR (Sigma), quantified by amino acid analysis (AAA) (Dana Farber Cancer Institute, Molecular Biology Core); *3)* 10 fmol/μl heavy-lysine (^{13}C and ^{15}N) labeled non-mutant tau-A152A peptide ($_{151}$IATPRGAAPPGQK$_{163}$), 10 fmol/μl heavy-lysine (^{13}C and ^{15}N) labeled mutant tau-A152T peptide ($_{151}$ITTPRGAAPPGQK$_{163}$) and 100 fmol/μl heavy-lysine (^{13}C and ^{15}N) labeled mutant tau-A152pT phospho peptide ($_{151}$IpTTPRGAAPPGQK$_{163}$) (synthesis and AAA by Thermo). Note, in a typical protein trypsin digestion, the peptide containing the site A152T is too short to be detected by MS, so instead we performed a LysC digestion that produces longer peptides, including the specific peptide containing the A152T variant (LysC digest in Figure 4A) for targeted MS measurement of non-mutant and A152T tau.

For the identification of non-mutant and mutant tau peptides, peptide mixtures were analyzed on a quadrupole Orbitrap tandem mass spectrometer (Q Exactive, Thermo) hyphenated with a micro-autosampler AS2 and a nanoflow HPLC pump (both Eksigent), coupled to an in-house packed C18 analytical column (Magic C18 particles, 3 μm, 200Å, Michrom Bioresource). Peptides were separated by a linear 30 min gradient from 95% buffer A (0.1% (v/v) formic acid in HPLC-H_2O) and 5% buffer B (0.2% (v/v) formic acid in acetonitrile) to 35% buffer B. A full mass spectrum with resolution of 70,000 (relative to an *m/z* of 200) was acquired in a mass range of 300-1500 m/z (AGC target 3 x 10^6, maximum injection time 20ms). The 10 most intense ions were selected for fragmentation via higher-energy c-trap dissociation (HCD, resolution 17,500, AGC target 2 x 10^5,

maximum injection time 250 ms, isolation window 1.6m/z, normalized collision energy 27%). The dynamic exclusion time was set to 20 s and unassigned/singly charged ions were not selected.

LC-MS/MS Data Processing

Q Exactive raw files were converted into *.mgf* data format using ProteoWizard. The spectra were centroided and filtered using ms2preproc to select the 6 most intense peaks in a 30 Th window. Collected spectra were searched against a *Homo sapiens* database (UniProt, version 11/01/2011) with ProteinPilotTM Software 4.5 Beta (Paragon Algorithm 4.5.0.0. 1575, Sciex). The following settings were applied: instrument type 'Orbi MS (1-3ppm)'; 'Urea denaturation'; 'rapid' search mode.

For the optimization of the FLEXITau SRM (Selected Reaction Monitoring) assay, in particular the addition of the peptides containing the A152T variant, *.xml* files were extracted from ProteinPilot and loaded into Skyline [version 2.6, MacCoss Lab Software, University of Washington (MacLean et al., 2010)], using cut off score of 0.5, to build a spectral library. The FLEXITau peptide tree was populated with transitions according to the spectral library. The transition lists were experimentally validated and optimized by initial LC-SRM (Liquid Chromatography - Selected Reaction Monitoring) measurements to select the most suitable transitions for quantification experiments (see below).

FLEXITau LC-SRM Measurements and Data Analysis

LC-SRM measurements of tau light-to-heavy (L/H) peptide ratios were performed as described previously (Mair et al., 2016); and data were analyzed and validated in Skyline. The FLEXITau SRM assay was optimized guided by a spectral library generated in-house through LC-MS/MS analysis (above). After optimization of the transition list, peptide mixtures were analyzed on a triple quadrupole mass spectrometer (5500 QTRAP, Sciex) using a micro-autosampler AS3 and a nanoflow UPLC pump (both Eksigent/Sciex), using the trap-elute chip system (cHiPLC nanoflex, Eksigent). Briefly, peptides were first loaded onto the trap-chip (200 μm x 75 μm, ChromXP C18-CL 3 μm 120A, Nano cHiPLC Eksigent) and then separated using a 120 min gradient from 95% buffer A (0.1% (v/v) formic acid in HPLC-H2O) and 5% buffer B (0.2% (v/v) formic acid in ACN) to 35% buffer B on the analytical column-chip (75 μm x 15 cm, ChromXP C18-CL 3 μm 120A, Nano cHiPLC Eksigent). The retention time window was set to 5 min and total scan time to 1.2 s, which ensured a dwell time over 20 ms per transition. First, a 1:10 dilution of each sample was analyzed to estimate relative quantities of tau in each sample. Subsequently, heavy tau standard peptides were added to the light peptide mix to achieve approximately a 1:1 L/H ratio of tau peptides. Spiked samples were measured in technical duplicates. SRM data were analyzed and validated in Skyline (MacLean et al., 2010). Peptide transitions were manually evaluated for variability, elution times, similarity between y-ion ratios, and interfering signals. Peak boundaries were inspected and reassigned as needed to ensure correct peak detection and accurate integration.

Absolute abundance of tau was calculated using the FLEX peptide L/H ratio as described before (Mair et al., 2016; Singh et al., 2009). Briefly, the L/H ratio of the FLEX peptide was used for quantification of heavy tau standard, which was then used to infer the total amount of endogenous tau in each sample. Tau amounts were calculated as fmol/μg of protein extract. Quantification of non-mutant and mutant tau peptides was achieved by determination of signal intensity of the light transitions relative to their Lysine-heavy counterparts originating from the spiked-in synthetic peptides. Relative amounts of non-mutant to mutant tau species (in %) were calculated for each time point of differentiation. For global FLEXITau analysis, in each sample the L/H ratio of each peptide was normalized by the average of the L/H ratio of the 3 peptides with highest ratio in that particular sample. First, average of normalized L/H ratio from the duplicate technical measurements was calculated, and subsequently the average of biological samples was taken. FLEXITau data was expressed as mean ±SD of normalized ratio of biological replicates. Statistical significance between control and tau-A152T samples was determined by the Student's t-test (accepted at the *p-value*<0.05 level).

Analysis of Protein Solubility by Detergent Fractionation

Sequential protein fractionation from differentiated neurons was performed according to published protocols (Guo and Lee, 2011, 2013; Kfoury et al., 2012). Briefly, cell pellets were resuspended in 5X the pellet volume with 1% Triton-X lysis buffer [1% (v/v) Triton X-100 in 50 mM Tris and 150 mM NaCl, pH 7.6] supplemented with phosphatase (Sigma) and protease (Roche) cocktail inhibitors, incubated on ice for 30 min and centrifuged at 20,000*g* for 30 min at 4°C. The supernatant was the Triton-fraction (T) and the pellet was washed once with 1% Triton X-100 lysis buffer, and later added to the total T-fraction. The pellet was resuspended in 2% SDS-lysis buffer [2% (w/v) SDS in 50 mM Tris and 150 mM NaCl, pH 7.6] using 1/3 of the volume used for the Triton-lysis buffer, incubated for 15 min, water sonicated for 5 min and centrifuged at 20,000*g* for 30 min at 20°C. The supernatant was the SDS-fraction (S). Protein concentration of the Triton fraction was determined with the Pierce BCA Protein Assay Kit (Thermo); and SDS-PAGE western blot was performed by loading 15 µg of T-fraction (in SDS-DTT loading buffer, DTT) and equal volume of the S-fraction onto pre-cast SDS-PAGE

(Novex, Invitrogen). The remainder of the procedures were performed as described in the western blot section. For quantification, band intensity is shown relative to respective GAPDH in T-fraction (Figure 5B).

Generation of *MAPT* Knockdown NPC Lines by CRISPR/Cas9 Genomic Engineering

The *MAPT* gene locus was targeted and disrupted by utilizing the Tau CRISPR/Cas9 KO Plasmid and Tau HDR Plasmid (Santa Cruz Biotechnology sc-400136/sc-400136-HDR), according to manufacturer's instructions. NPCs (19-L5-RC6) at 80% confluency were co-electroporated with the two plasmids (3μg DNA/plasmid) using the Amaxa Biosystems Nucleofector II AAD-1001N and Amaxa Human Stem Cell Nucleofector Kit 2 (Lonza), according to manufacturer's instructions. Upon 24h recovery, puromycin (Sigma) selection was initiated (1μg/mL in DMEM/F12-B27 media with E.F.H.) to obtain RFP^+ only cells, which can occur when cells have at least one or both of the *MAPT* alleles disrupted. During puromycin selection, small colonies of RFP^+ cells were selected (by microscopy assessment, Zeiss Axiovert) and expanded, to originate three of the new lines: 19-L5-RC6;*MAPT*-Kd1, 19-L5-RC6;*MAPT*-Kd2 and 19-L5-RC6;*MAPT*-Kd3. Upon 4-weeks of differentiation, expression of the *MAPT* gene was assessed by RT-PCR as described above, revealing that gene expression was down-regulated by ≥60% in the population of neurons in culture (*not shown*). By Western blot analysis of total tau levels in 4-week differentiated neurons (by TAU5 and DA9 antibodies), protein expression was determined to be down-regulated by >80% in the population of neurons in culture, relative to the original 19-L5-RC6 4-week differentiated neurons. In the end, the line chosen for further studies was 19-L5-RC6;*MAPT*-Kd3, which revealed the lowest level of tau expression (most efficient knockdown). 19-L5-RC6;*MAPT*-Kd3 differentiated neurons at 8 weeks were examined for morphology (Zeiss Axiovert, phase imaging) and cellular viability (Alamar Blue Cell viability reagent, Life Technologies).

Compound Treatment and Viability Assays

For viability assays (96-well plate format), the following compounds were added to 2-week or 8-week differentiated neural cultures, directly into the media: rotenone (Enzo Lifesciences), piericidin-A (Enzo Lifesciences), glutamate (Sigma), NMDA (N-Methyl-D-Aspartic Acid; Enzo Lifesciences), amyloid-beta(1-42) (Enzo Lifesciences), MG132 (Calbiochem InSolution), epoxomicin (Enzo Lifesciences). Viability was measured 24h later, with the Alamar Blue Cell viability reagent (Life Technologies), according to manufacturer's instructions. Readings were done in the EnVision Multilabel Plate Reader (Perkin Elmer). For rapamycin (Enzo LifeSciences) pre-treatment (8-week differentiated neurons, 6-well plate), 5μM RAP or vehicle (DMSO) alone was added to the cultures for 8h. Then, the stressor compounds were added directly to the same media for a total of 24h incubation, at which point cell viability was measured as described above.

To test activation of autophagy (LC3B-II), and consequent effect on tau levels (Figure S6N-P), by rapamycin (Enzo LifeSciences) treatment, 5-week differentiated neurons (6-well plates) were treated with the compound (2μM or 5μM) or vehicle (DMSO) alone for 24h, and collected for Western blot analysis as described above.

Supplemental References

Elliott, A.M., Elliott, K.A., and Kammesheidt, A. (2010). High resolution array-CGH characterization of human stem cells using a stem cell focused microarray. Mol Biotechnol *46*, 234-242.

Koch, P., Opitz, T., Steinbeck, J.A., Ladewig, J., and Brustle, O. (2009). A rosette-type, self-renewing human ES cell-derived neural stem cell with potential for in vitro instruction and synaptic integration. Proc Natl Acad Sci U S A *106*, 3225-3230.

MacLean, B., Tomazela, D.M., Shulman, N., Chambers, M., Finney, G.L., Frewen, B., Kern, R., Tabb, D.L., Liebler, D.C., and MacCoss, M.J. (2010). Skyline: an open source document editor for creating and analyzing targeted proteomics experiments. Bioinformatics *26*, 966-968.

Takahashi, K., Tanabe, K., Ohnuki, M., Narita, M., Ichisaka, T., Tomoda, K., and Yamanaka, S. (2007). Induction of pluripotent stem cells from adult human fibroblasts by defined factors. Cell 131, 861-872.

Takahashi, K., and Yamanaka, S. (2006). Induction of pluripotent stem cells from mouse embryonic and adult fibroblast cultures by defined factors. Cell *126*, 663-676.

Villa-Diaz, L.G., Kim, J.K., Lahann, J., and Krebsbach, P.H. (2014). Derivation and long-term culture of transgene-free human induced pluripotent stem cells on synthetic substrates. Stem Cells Transl Med *3*, 1410-1417.

Wisniewski, J.R., Zougman, A., Nagaraj, N., and Mann, M. (2009). Universal sample preparation method for proteome analysis. Nat Methods *6*, 359-362.

Zheng, J., and Bizzozero, O.A. (2010). Reduced proteasomal activity contributes to the accumulation of carbonylated proteins in chronic experimental autoimmune encephalomyelitis. J Neurochem *115*, 1556-1567.